Insights from structure-activity relationships and the binding mode of peptidic α-ketoamide inhibitors of the malaria drug target subtilisin-like SUB1

Alice Legru, Fernando Batista, Anna Puszko, Anthony Bouillon, Manon Maurel, Mariano Martinez, Abdelaziz Ejjoummany, Laura Ortega Varga, Pauline Adler, Ariel E Mechaly, et al.

▶ **To cite this version:**

Alice Legru, Fernando Batista, Anna Puszko, Anthony Bouillon, Manon Maurel, et al.. Insights from structure-activity relationships and the binding mode of peptidic α-ketoamide inhibitors of the malaria drug target subtilisin-like SUB1. European Journal of Medicinal Chemistry, 2024, 269, pp.116308. 10.1016/j.ejmech.2024.116308 . hal-04727940

HAL Id: hal-04727940
https://hal.science/hal-04727940v1

Submitted on 9 Oct 2024

HAL is a multi-disciplinary open access archive for the deposit and dissemination of scientific research documents, whether they are published or not. The documents may come from teaching and research institutions in France or abroad, or from public or private research centers.

L'archive ouverte pluridisciplinaire **HAL**, est destinée au dépôt et à la diffusion de documents scientifiques de niveau recherche, publiés ou non, émanant des établissements d'enseignement et de recherche français ou étrangers, des laboratoires publics ou privés.

HAL Authorization

Insights from structure-activity relationships and the binding mode of peptidic α-ketoamide inhibitors of the malaria drug target subtilisin-like SUB1

Alice Legru[a,1,#], Fernando A. Batista[b,#], Anna K. Puszko[a,2], Anthony Bouillon[b], Manon Maurel[a,3], Mariano Martinez[b], Abdelaziz Ejjoummany[a], Laura Ortega Varga[c,4], Pauline Adler[a], Ariel Méchaly[d], Margot Hadjadj[a,5], Piotr Sosnowski[e,6], Gérard Hopfgartner[e], Pedro M. Alzari[b], Arnaud Blondel[c], Ahmed Haouz[d], Jean-Christophe Barale[b,‡,*] and Jean-François Hernandez[a,‡,*]

[a]*Institut des Biomolécules Max Mousseron (IBMM), CNRS, Univ Montpellier, ENSCM, Montpellier, France.* [b]*Structural Microbiology, UMR3528, Institut Pasteur, CNRS, Université de Paris, Paris, France.* [c]*Structural Bioinformatic, UMR3528, Institut Pasteur, CNRS, Université de Paris, Paris, France.* [d]*Cristallography platform-C2RT, UMR3528, Institut Pasteur, CNRS, Université de Paris, Paris, France.* [e]*Department of Inorganic and Analytical Chemistry, University of Geneva, CH-1211 Geneva, Switzerland.*

Present address:
[1] Oxeltis, Cap Gamma, 1682 rue de la Valsière, 34086 Montpellier, France.
[2] Laboratory of Peptides, Faculty of Chemistry, University of Warsaw, Pasteura 1, 02-093 Warsaw, Poland.
[3] SpiroChem, Rosental area, WRO-1047-3, Mattenstrasse 22, 4058 Basel, Switzerland.
[4] Alzheimer's Research UK Oxford Drug Discovery Institute, Centre for Medicines Discovery, Nuffield Department of Medicine, University of Oxford, Oxford, OX3 7FZ, UK.
[5] Department of Pharmacology and Physiology, University of Sherbrooke, Sherbrooke, J1H 5N, Quebec, Canada.
[6] Department of Bioanalytics, Medical University of Lublin, Jaczewskiego 8b, 20-090 Lublin, Poland.

[#] These authors contributed equally to this work.
[‡] These authors contributed equally to the supervision of this work.

*Corresponding authors: jean-francois.hernandez@umontpellier.fr, jean-christophe.barale@pasteur.fr

Abbreviations: *Ac*, acetyl; *αKA*, α-ketoamide; *All*, allyl; *ACT,* artemisinin-based combination therapy*; ART,* artemisinin*; BOC, tert*-butyloxycarbonyl*; BOP,* benzotriazole-1-yl-oxy-tris-(dimethylamino)-phosphonium hexafluorophosphate; *tBu, tert*-butyl*; Cpg,* cyclopentylglycine*; Dab*, 2,4-diaminobutyric acid; *Dabsyl*, 4-dimethylaminoazobenzene-4'-sulfonyl; *Dap*, 2,3-diaminopropionic acid; *DCM*, dichloromethane; *DIEA*, diisopropylethylamine; *DMF*, dimethylformamide; *DMP*, Dess-Martin Periodinane; *DMSO*, dimethylsulfoxide; *DODT*, 3,6-dioxa-1,8-octanedithiol; *EDANS*, 8-(2-aminoethylamino)-1-naphthalenesulfonic acid; *EtOAc*, ethyl acetate; *Fmoc*, fluorenylmethyloxycarbonyl; *FRET*, Fluorescence Resonance Energy Transfer; *HATU*, 1-[[(dimethylamino)methylene]-*N*-methylmethanaminium]-1*H*-1,2,3-triazolo[4,5-b]pyridinium-3-oxide hexafluorophosphate; *Hex*, hexane; *LC-MS*, liquid chromatography coupled to mass spectrometry; *Mtt*, 4-methyltrityl; *NMP*, *N*-methyl-pyrrolidone; *PDB*, protein data bank; *Pip*, piperidine; *PS*, polystyrene; *RMSD*, root mean square deviation; *RP-HPLC*, reverse phase high performance liquid chromatography; *SAR*, structure-activity relationships; *TEA*, triethylamine; *TFA*, trifluoroacetic acid; *TFE*, trifluoroethanol; *THF*, tetrahydrofuran; *TIS*, triisopropylsilane; *TNBS*, trinitrobenzenesulfonic acid; *Tza*, tetrazolylalanine.

ABSTRACT.

Plasmodium multi-resistance, including against artemisinin, seriously threatens malaria treatment and control. Hence, new drugs are urgently needed, ideally targeting different parasitic stages, which are not yet targeted by current drugs. The SUB1 protease is involved in both hepatic and blood stages due to its essential role in the egress of parasites from host cells, and, as potential new target, it would meet the above criteria. We report here the synthesis as well as the biological and structural evaluation of substrate-based α-ketoamide SUB1 pseudopeptidic inhibitors encompassing positions P4-P2'. By individually substituting each position of the reference compound **1** (MAM-117, Ac-Ile-Thr-Ala-AlaCO-Asp-Glu(Oall)-NH_2), we better characterized the structural determinants for SUB1 binding. We first identified compound **8** with IC_{50} values of 50 and 570 nM against Pv- and PfSUB1, respectively (about 3.5-fold higher potency compared to **1**). Compound **8** inhibited *P. falciparum* merozoite egress in culture by 37% at 100 μM. By increasing the overall hydrophobicity of the compounds, we could improve the PfSUB1 inhibition level and antiparasitic activity, as shown with compound **40** (IC_{50} values of 12 and 10 nM against Pv- and PfSUB1, respectively, IC_{50} value of 23 μM on *P. falciparum* merozoite egress). We also found that **8** was highly selective towards SUB1 over three mammalian serine peptidases, supporting the promising value of this compound. Finally, several crystal 3D-structures of SUB1-inhibitor complexes, including with **8**, were solved at high resolution to decipher the binding mode of these compounds.

Keywords: Malaria; SUB1 inhibitors; α-ketoamides; pseudopeptides; SAR; crystal structures.

1. Introduction

In 2021, 247 million cases of malaria and 619,000 deaths were reported worldwide, representing a significant decline in mortality since 2000, partly due to the massive and coordinated use of artemisinin (ART)-based combination therapy (ACT) [1]. However, the decrease rate has been slower since 2014 and an increase is observed since 2020, which is presumably related to service disruptions during the COVID-19 pandemic and shows the fragility of progress in malaria control. Importantly, the efficacy of ACTs in South-East Asia has been worryingly decreasing since 2008, due to the emergence of ART-resistance, thus impacting the global strategy to fight this major infectious disease [2,3]. The recent emergence of ART-resistant *P. falciparum* in Africa, where 95% of the deaths occurred, in combination with *Anopheles* resistance to insecticides, worringly menaces the control of malaria burden [4-7]. Therefore, this situation reinforces the need for the development of new antimalarials, particularly targetting novel pathways essential at different stages of *Plasmodium* life cycle. Targeting *Plasmodium* hepatic and blood schizonts is a priority mentioned by Medicines for Malaria Venture (MMV) [https://www.mmv.org], since these stages correspond to parasite asexual multiplication in humans. The egress of merozoites from schizont-infected hepatocytes and erythrocytes is a yet untargeted essential step that strictly depends upon a cascade of parasite proteases, thus defining these enzymes as potential novel drug targets distinct from those addressed by existing anti-malarials.

The *Plasmodium* subtilisin-like protease 1 (SUB1) [8] is a key player during the finely regulated egress of merozoites from host-infected cells and has been defined as a highly promising target. Indeed, SUB1 is crucial for merozoites egress from both infected erythrocytes [9] and hepatocytes [10,11], and their subsequent invasion into new erythrocytes [12]. It has also recently been shown to be essential for the egress of male gametes, thus being involved in *Plasmodium* transmission to its vector, the *Anopheles* mosquito [13]. This SUB1 multi-stages pivotal role implies that SUB1-specific inhibitors would have both prophylactic, therapeutic and transmission blocking properties, and therefore would fulfil the criteria expected for the next generation of anti-malarials, i.e. targeting all *Plasmodium* life cycle phases in human [14,15]. Furthermore, SUB1 active site is similar to bacterial subtilisins and thus significantly differs from human serine peptidases, which should be favourable for inhibitor selectivity [16,17]. In addition, an unusual feature of SUB1 is that its binding site allows interaction with not only the non-prime but also the prime side residues of its substrates, which significantly broadens the possibilities of designing effective inhibitors [18,19]. Finally, the crystal structures of full-length SUB1 from *P. vivax* ($PvS1_{FL}$) [20] and *P. falciparum* ($PfS1_{FL}$) [21], the two most devastating human-infecting parasites, have been reported. Both structures showed the SUB1 catalytic domain in complex with its cognate propeptide. Furthermore, the 3D structures of the active propeptide-free PvS1 catalytic domain ($PvS1_{CD}$) and of

its complex with a substrate-derived pseudopeptidic inhibitor MAM-117 (here named reference compound **1**, see below) have recently been described [19]. The Pf/PvS1 structures showed that both active sites are virtually identical, which is consistent with the observed similar inhibition (K_i values of ≈ 10 μM) of both enzymes by the substrate-based inhibitor, JMV5126 [20].

Several SUB1 inhibitors have been discovered by following two approaches. The first one was the random screening of small molecule libraries that led to identify only poorly effective inhibitors with negligible prospects for optimization [9,17,22-24]. The more rational second approach aimed at developping structure- and mechanism-based pseudopeptidic inhibitors derived from (i) SUB1 native substrates and containing an electrophilic ketone (i.e. α-ketoamide and difluoromethylketone) [18,20,25,26] or (ii) natural serine protease inhibitors [27,28]. However, despite some of these compounds had micromolar range inhibitory activity, most of them were devoid of significant effect on parasite growth *in vitro*, possibly because of low stability and/or cell permeability. A series of peptide-boronates showing PfS1 inhibitory potencies in the nanomolar range and able to inhibit *P. falciparum* merozoites egress at the micromolar range has recently been reported [29,30], supporting the promising potential of SUB1 as an anti-malaria target. Whereas these compounds were shown to be selective toward serine peptidases of the S1 family [31], they do not contain P' residue, which could increase the risk of limited selectivity on other enzymes. Also, nothing is known regarding their potential impact on *P. falciparum* stages that lack SUB1 to evaluate eventual off-target antiparasitic effect.

Following the report of the pseudopeptide JMV5126 (Figure 1) [20], we pursued the development of inhibitors containing the α-ketoamide (αKA) serine peptidase targeting warhead. In the αKA group, the electrophilic ketone located between the P1 and P1' residues of the inhibitor forms a reversible covalent adduct with the hydroxyl group of the catalytic serine of the peptidase, mimicking the substrate/enzyme transition state and allowing reaching nanomolar levels of inhibition [32]. Moreover, such inhibitors are easily chemically assembled using solid phase strategy and they can span both S and S' sides of the binding cleft, allowing more specific interaction due to the presence of P' residues as specified above. The αKA group has largely been used in serine peptidase inhibitors and could lead to drugs as Telaprevir, an orally active anti-HCV serine protease agent, marketed to treat Hepatitis-C [32].

JMV5126 encompassed the positions P6-P4' of the main SUB1-promoted maturation site present within the Serine Repeat Antigen 4 (SERA4), a putative cysteine peptidase involved in merozoite egress from host infected cells [9,33] (Figure 1). With K_i values in the 10 μM range against both *Pf*- and *Pv*S1, JMV5126 was about 10-fold less potent than other reported αKA SUB1 inhibitors with an Ala side chain at the P1 position [25]. A plausible reason is the existence of an equilibrium

between the active α-ketoamide form and an inactive cyclic form arising from the reaction of the side chain of Gln with the α-keto group [25] (Figure 1). Therefore, to avoid this issue, we replaced the Gln P1 residue by Ala, which precursor is also much easier to synthesize. We also reduced the peptidic length to span the P4-P2' positions and replaced the P2' Asp residue by an allyl-protected Glu, leading to the recently reported reference compound **1** (MAM-117) (Figure 1) [19].

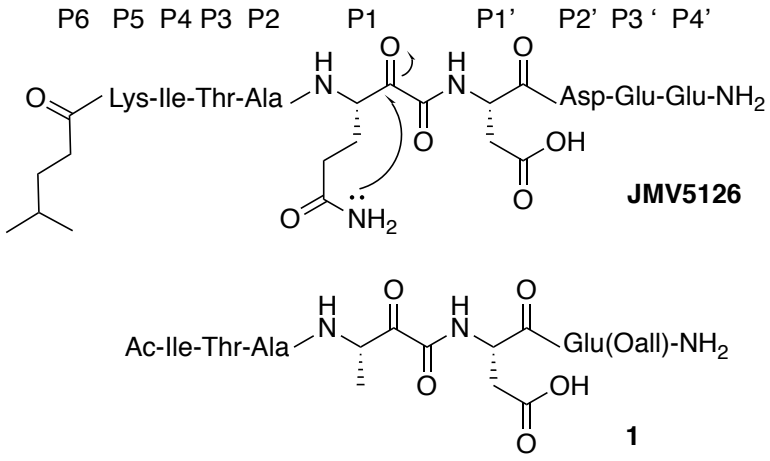

Figure 1. Structures of JMV5126 showing the putative intramolecular reaction between Gln side chain and the α-keto group [25], and of compound **1** (MAM-117), the reference compound of the series presented herein. Both compounds are derived from the PfSERA4 maturation site ^{306}LKITAQ↓DDEE^{315}.

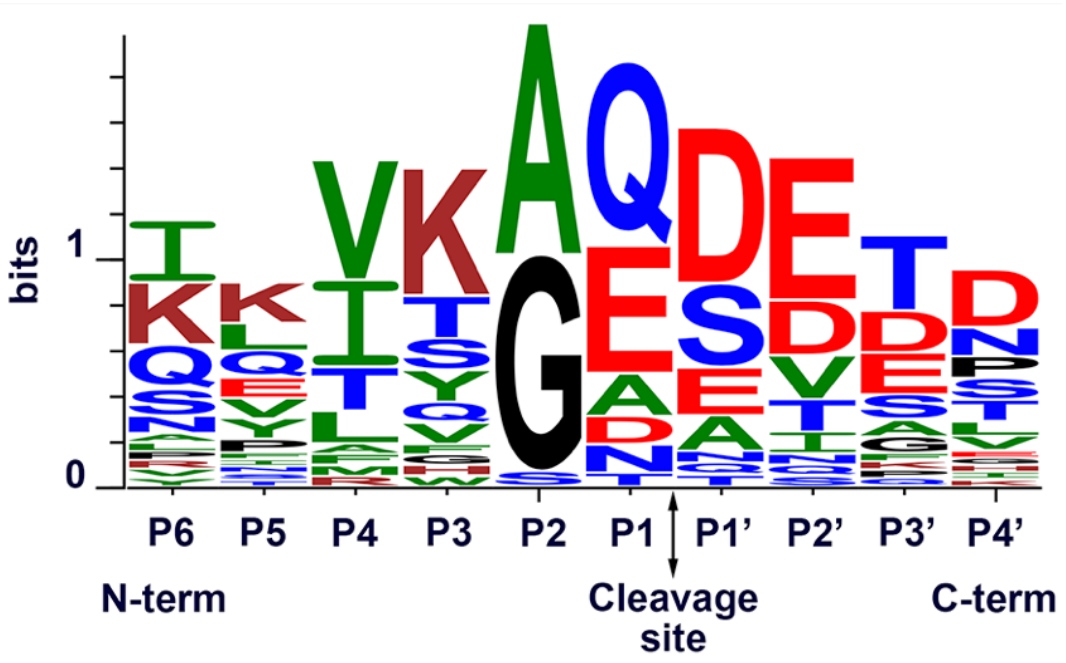

Figure 2. Sequence logo of cleavage site of SUB1 native substrates, including SUB1 auto-maturation and *P. falciparum* MSP1 cleavage sites, also the ones of *P. falciparum* and *P. vivax* families of SERA [34,35].

Considering the consensus substrate recognition motif of SUB1 (Figure 2) [28], we explored each position of compound **1** to identify more favourable residues for SUB1 inhibition and/or for the inhibition of *P. falciparum* merozoite egress. A significant improvement in inhibitory potencies

with IC_{50} values in the 10 nM range against Pv- and PfS1 was observed when introducing a cyclopentylglycine (Cpg) at the P4 and P2' positions. In addition, this increase in potency toward SUB1 correlated with increased antiparasitic activity *in vitro*. Finally, three novel crystal structures of $PvS1_{CD}$/inhibitor complexes are presented.

2. Results and Discussion

2.1. Synthesis

2.1.1. Synthesis of amino acid derivatives

The α-ketoacyl residues were obtained from the Fmoc-protected corresponding β-amino-α-hydroxy-acid precursors (norstatine-like derivatives) or from the alanine-derived α-ketoacid protected with 1-(4-methoxyphenyl)-2,2-dimethylpropane-1,3-diol [36]. We also prepared the Fmoc-protected tetrazolylalanine derivative as a bioisoster of aspartic acid.

*2.1.1.1. Synthesis of norstatine-like derivatives **VII** and **IX**.* The precursor of the α-ketoacyl residue with an alanine side chain, **VII** ((3*S*)-3-(Fmoc-amino)-2-hydroxybutanoic acid) was obtained in four steps from Fmoc-Ala-OH (Scheme 1). The Fmoc-protected amino acid was coupled with *N,O*-dimethylhydroxylamine to yield the Weinreb amide **I**, which was reduced to the aldehyde **III** using $LiAlH_4$. The aldehyde was reacted with acetone cyanohydrin giving compound **V**, which was converted to the norstatine derivative **VII** in acidic conditions.

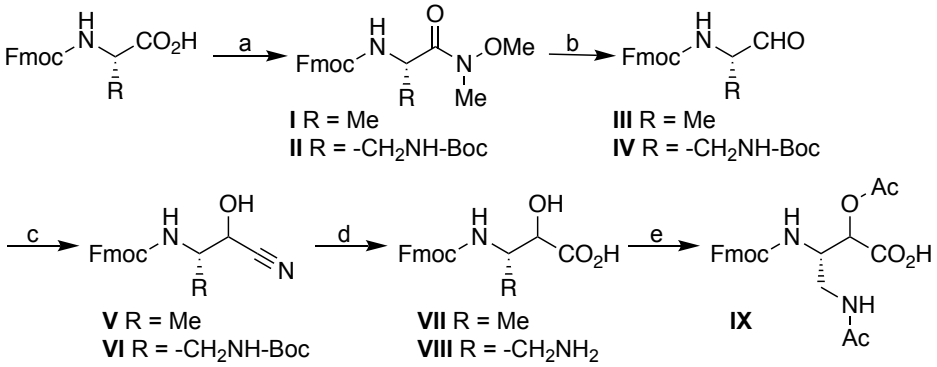

Scheme 1. Synthesis of norstatine derivatives. Reagents and conditions. *(a) HN(OMe)Me,HCl (1.3 equiv.), HATU (1.3 equiv.), DIEA (1.5 equiv.), DCM, 16h (I: 91%; II: 73%); (b) $LiAlH_4$ (1.5 equiv.), THF, -15 °C, 1h; (c) acetone cyanohydrin (3 equiv.), TEA (0.6 equiv.), DCM, 16h (two steps: V: 52%; VI: 90%); (d) conc. HCl/dioxane (2:1), reflux, 8h (VII: 59%; VIII: 47%); (e) Ac_2O (3 equiv.), DIEA (4 equiv.), DCM, 0 °C, 30 min (58%).*

We also introduced at the P1 position a side-chain analogue of glutamine, which possessed the same atomic composition and an amide bond. Its precursor **IX** ((3*S*)-2-acetyloxy-4-acetamido-3-(Fmoc-amino)-butanoic acid) was prepared from protected 2,3-diaminopropanoic acid, Fmoc-Dap(Boc)-OH (Scheme 1). The first four steps were similar as for compound **VII** and yielded the

side-chain deprotected compound **VIII**. Treatment with acetic anhydride led to acetylation of both side-chain amine and hydroxyl groups (compound **IX**).

*2.1.1.2. Fmoc-protected (L)-tetrazolylalanine (Fmoc-Tza-OH) **XI***. Due to the acidic property of the aspartyl residue present at position P1' of the reference compound **1**, which might hamper cell membrane penetration, we considered replacing the side-chain carboxylic group by its tetrazole bioisostere [37]. Therefore, we synthesized the Fmoc-protected tetrazole analogue of Asp (**XI**) [38]. Compound **XI** was prepared from Fmoc-Asn-OtBu in three steps (Scheme 2). After dehydration of the side-chain amide using cyanuric chloride, the cyano compound **X** was treated with tributyltin azide, followed by acidic cleavage of the *tert*-butyl ester, to yield tetrazole derivative **XI** [39,40].

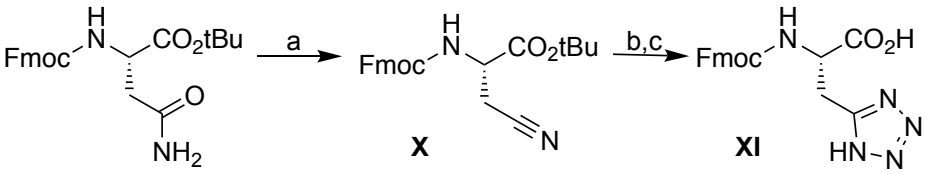

Scheme 2. Synthesis of Fmoc-Tza-OH **XI**. Reagents and conditions. *(a) Cyanuric chloride (1.3 equiv.), DMF, 0 °C, 30 min (60%); (b) (i) n-Bu_3SnN_3, 80 °C, 48h (ii) 5N HCl, 1h; (c) 50% of TFA/TIS/H_2O (95:2.5:2.5) in DCM, 1h (88%).*

2.1.2. Peptide synthesis

All peptidic compounds (Tables 1 and S1) were assembled on the solid phase using a Fmoc-protected Rink amide resin, following the Fmoc strategy and using HATU (*N*-[(dimethylamino)-1*H*-1,2,3-triazolo-[4,5-*b*]pyridin-1-ylmethylene]-*N*-methylmethanaminium hexafluorophosphate *N*-oxide) as the coupling agent. In the case of the protected alanine-derived α-ketoacid, this derivative was introduced with BOP (benzotriazole-1-yl-oxy-tris-(dimethylamino)-phosphonium hexafluorophosphate) instead of HATU. When a norstatine-like precursor (i.e. **VII**, **IX**) was used, its hydroxyl group was oxidized by treatment with Dess-Martin Periodinane (DMP) after peptide assembly and before acidic cleavage to yield the α-ketoacyl residue (Scheme 3).

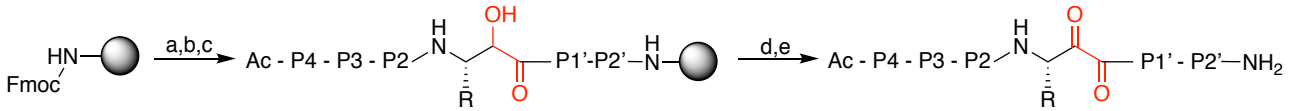

Scheme 3. General solid-phase peptide synthesis pathway. Reagents and conditions. *(a) Pip/DMF (20:80), rt, 10 + 25 min; (b) Fmoc-AA-OH (3 equiv.), HATU (3 equiv.), DIEA (4 equiv.), DMF, rt, 2h; (c) in the case of **IX**-derived norstatine residue: Na_2CO_3 (2 eq.) in THF/H_2O (7:3), rt, 1h; (d) DMP (3 equiv.), DCM, rt, 2 x 3h; (e) TFA/TIS/H_2O (95:2.5:2.5), rt, 2h. Global yields are presented in Table S1.*

In the case of the **IX**-derived norstatine-like residue, which hydroxyl group is acetylated, the acetyl was prealably removed by treatment with 2 eq. Na_2CO_3 in THF/H_2O (7:3). When a protected α-

ketoacyl residue was present, the peptide-resins were cleaved and deprotected with a mixture of TFA/TIS/H_2O/DODT (91:3:3:3) [36].

2.2. Biological evaluation and study of structure-activity relationships

2.2.1. Inhibition of SUB1 recombinant enzymes and inhibition assay of P. falciparum *merozoite egress from human erythrocytes* in vitro

The inhibitory potency of the compounds was assessed on purified recombinant SUB1 proteins using a previously described enzymatic assay, which follows the digestion of a FRET-based peptide substrate [17]. All compounds were tested against *P. vivax* full length SUB1 ($PvS1_{FL}$) and its free catalytic form $PvS1_{CD}$, prepared as previously described [19]. Overall, the IC_{50} values measured for both PvS1 forms were similar. $PvS1_{FL}$ inhibition data are shown in Table 1 while IC_{50} values for $PvS1_{CD}$ (compared with $PvS1_{FL}$) are presented in Table S2. The yield of $PfS1_{FL}$ production being significantly lower than the one of $PvS1_{FL}$, only selected compounds have also been tested on $PfS1_{FL}$ (Table 1). Finally, the most potent SUB1 inhibitors were selected to assess their ability to inhibit the egress of *P. falciparum* merozoites from human erythrocytes *in vitro* as previously described (T0-T8 assay, Figure S1A) [41]. Briefly, infected erythrocytes containing mature schizonts (T0) were incubated with the compounds (at 100 and/or 25 μM), and newly invaded rings were counted eight hours later (T8) by cytometry. For this experiment, we prepared and used as a reference the compound named "49c", which has been described to prevent merozoite egress via inhibiting the parasite aspartyl proteases plasmepsins IX/X thought to participate in SUB1 activation [42,43]. As expected, "49c" fully inhibited merozoite egress with an IC_{50} value of 1.1 nM (Table 1).

The present study of structure-activity relationships (SAR) was based on the reference inhibitor **1**, which encompasses positions P4-P2' of SUB1 maturation site of SERA4 where the P1 Gln and P2' Asp residues have been replaced by the α-ketoacyl derivative of Ala and an allyl-protected Glu residue, respectively. Compound **1** inhibited $PvS1_{FL}$ and $PfS1_{FL}$ with IC_{50} values of 0.18 and 1.95 μM, respectively (Table 1). The 10-fold lower efficiency toward $PfS1_{FL}$ was unexpected since both active sites are highly conserved and their substrate profiles are similar [17,18,20]. This difference could be due to the inhibition mode of the αKA compounds. Indeed, these inhibitors react with the catalytic serine to form a covalent but reversible hemi-ketal adduct and the IC_{50} at least partially depends on the half-life of this covalent complex, which could be less stable in the case of PfS1. Compound **1** showed a poor 13% inhibition of merozoite egress at 100 μM.

To guide the SAR study, we took in consideration a map of structural preferences at each position, derived from the analysis of SUB1 native substrates: while no clear preference can be associated

with the P3 position, P4 and P2 residues should be hydrophobic and small, respectively, while P1, P1' and P2' residues are mainly polar or acidic [28,44] (Figure 2). The crystallographic structures of Pf- and PvS1 indicate that the preferred type of residues at P4, P2, P1 and P1' is related to well-defined corresponding subsites in the substrate binding site [20,21]. To better define the structural requirements at these positions and to possibly obtain more efficient analogues, we examined each position by introducing close and/or bulkier residues (Figure 3, Table 1). As structurally close residues can exhibit slightly different physico-chemical properties, hydrophobicity and bulkiness, these changes may lead to increased affinity. We also explored the P3 and P2' positions to improve the bioavailability and/or stability of these compounds and thus their activity in parasite culture.

2.2.1.1. Position P4. In SUB1 substrates, the P4 position is highly important for enzyme binding and is preferentially occupied by an aliphatic residue such as Val or Ile (Figure 2). Compound **1** possesses an Ile residue that has been replaced by various unnatural amino acids with similar but bulkier and more hydrophobic side chains (Figure 3, Table 1). Most compounds (**2**-**5**, **7**) appeared as potent as **1** against PvS1 activities with IC_{50} values comprised between 0.20 and 0.46 μM. Compound **5** also inhibited PfS1 in the same range as **1**. In addition, compounds **3**, **5** and **7** did not show better antiparasitic activity. Compound **6**, which possesses the bulkiest P4 residue in this series, cyclohexylalanine (Cha), was around 20-fold less efficient against PvS1 and PfS1 than **1** and its close analogue **5** with cyclohexylglycine (Chg), indicating that the Cha side chain was too large to properly fit into the SUB1' S4 subsite. In contrast, compound **8** with a cyclopentylglycine (Cpg) residue at P4 was around 4-fold more potent against PvS1 and PfS1 activities **(**IC_{50} values of 50 and 570 nM, respectively) than **1** and its closest analogue **5**. It is remarkable that a minor structural difference (i.e. a CH_2 between Chg in **5** and Cpg in **8**) led to such significant improvement. The reason of this effect is not yet fully understood, but clearly Cpg, despite an additional carbon over Ile, is made compact by its cyclization and it can "point" favorably in the P4 cavity. It is interesting to note that compound **2** with an Aep, which side chain has the same number of carbons as Cpg but can be considered as an open cyclopentyl moiety, is close to 10-fold less potent than **8** on PvS1. It confirms that the cyclic restraint is essential for the observed effect. This is consistent with similar results we previously obtained in another protein/ligand binding context by replacing an essential Leu residue by a Chg [45]. As illustrated by the X-ray structures of the complexes (see below), the P4 residues Ile (compound **1** [19]) and Cpg (compound **8**) fit similarly the S4 subsite (Figure S6B). One hypothesis is that the constrained and less flexible Cpg side chain could impact the binding by reduction of the number of side chain conformations in the free form (entropic contribution). A similar result was obtained by E. Lidumniece et al., who also reported the interest of Cpg at P4 position to inhibit PfS1 with peptide boronate compounds [29].

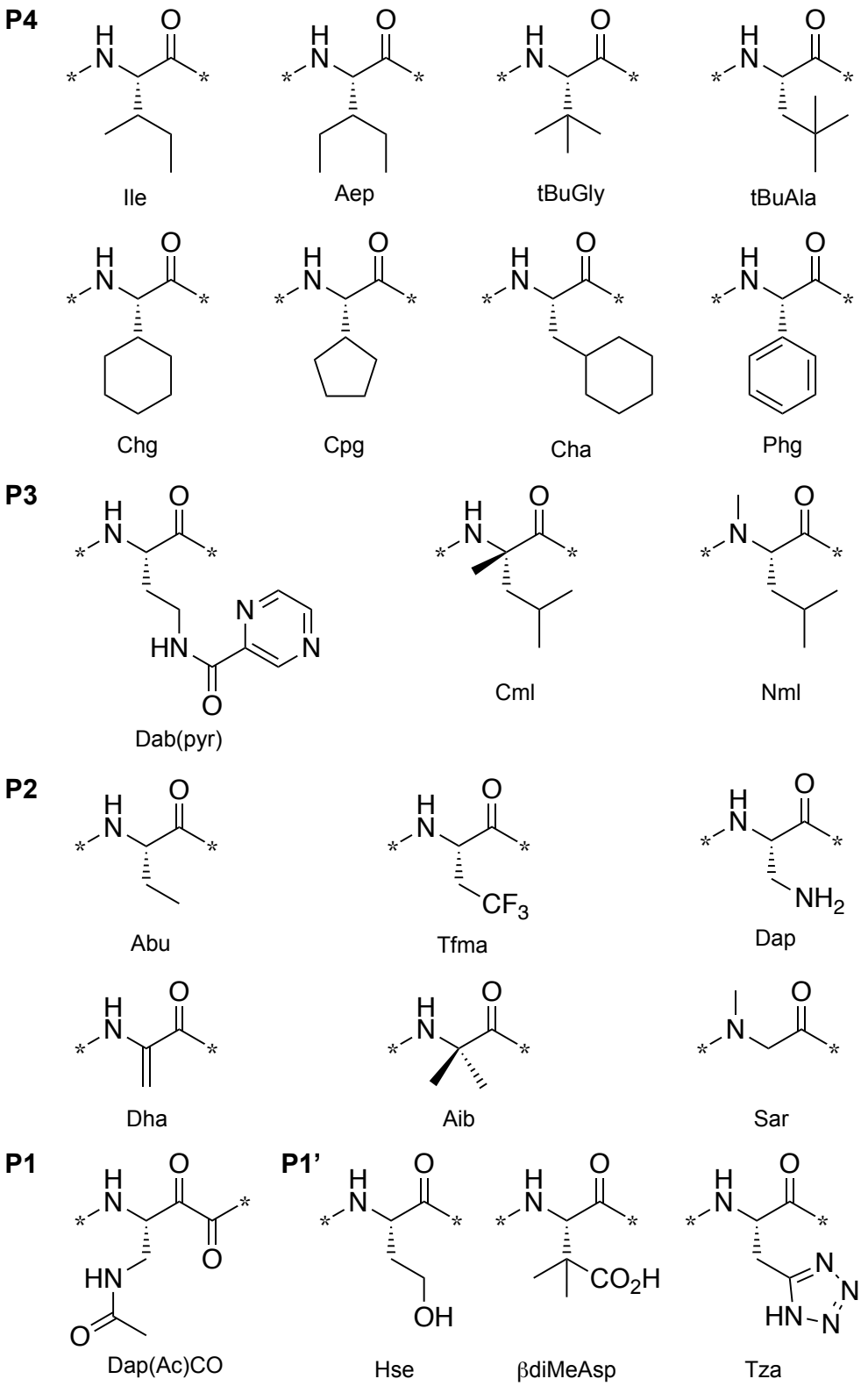

Figure 3. Structure of the non-proteinogenic amino acid residues used in this study. The positions where they have been individually introduced are indicated. The P4 Ile residue is included for comparison with residues introduced at this position. Abu, 2-aminobutyryl; Aep, 2-amino-3-ethyl-pentanoyl; Aib, α-aminoisobutyryl; tBuAla, *tert*-butyl-Ala; tBuGly, *tert*-butyl-Gly; Cha, cyclohexyl-Ala; Chg, cyclohexyl-Gly; Cml, Cα-methyl-Leu; Cpg, cyclopenbtyl-Gly; Dab(pyr), N^4-pyrazinoyl-2,4-diamino-butyryl; Dap, 2,3-diamino-propanoyl; Dha, dehydroalanine; Hse, homoserine; Nml, *N*-methyl-Leu; Phg, phenylglycine; Sar, sarcosine; Tfma, trifluoromethyl-Ala; Tza, tetrazole-Ala.

As observed for compound **1**, compounds **5**, **6** and **8** showed a constant 9- to 10-fold lower inhibitory potency against PfS1 than toward PvS1. In the case of compound **8**, it means that the replacement of Ile by Cpg improved as well (3- to 4-fold) the activity against PfS1 (IC_{50} value of 0.57 μM vs 1.95 μM for **1**). Interestingly, the higher potency of **8** against PfS1was accompanied by a 3-fold increase in the antiparasitic activity.

Overall, a Cpg at the P4 position was found to be of high interest for both PvS1 and PfS1 inhibition, and therefore this residue was used during the study of other positions. Finally, in this series, the best PfS1 inhibitor **8** was also the most potent in the T0-T8 assay, supporting that the observed merozoite egress inhibition correlates with a potent inhibition of SUB1 enzymatic activity.

2.2.1.2. Position P3. SUB1 has no clear preference at the P3 position of its substrates (Figure 2). This observation is consistent with the crystal structures of $PfS1_{FL}$ and of $PvS1_{CD}$ in complex with MAM-117, which, respectively, showed that the P3 side chain of the bound pro-peptide (i.e. serine) and of MAM-117 (i.e. threonine) points outside the enzyme binding cleft [19,21]. Therefore, this position might be modified to improve cell penetration as well as metabolic stability.

The threonine residue at P3 position of compound **1** was first substituted with the hydrophobic and aromatic Trp residue (**9**), and basic residues like Lys (**10**) and Dab loaded with a pyrazinoyl moiety (Figure 3) (**11**) to enhance membrane crossing and intracellular accumulation. Unfortunately, although these compounds inhibited PvS1 similarly to **1**, none of them showed improved antiparasitic activity (Table 1). We also modified compound **8** by introducing a second Cpg residue at position P3. The corresponding compound **12** displayed a slightly lower IC_{50} value against PvS1 but showed a 6-fold more potent PfS1 inhibition. In fact, this compound similarly inhibited both PvS1 and PfS1 (IC_{50} values of 0.08 and 0.10 μM, respectively). This higher PfS1 inhibition might explain that **12** was slightly more potent than **8** in the merozoite egress assay. Replacing Cpg by a Tyr residue at P3 (**13**) led to similar results, suggesting that a bulkier and/or more hydrophobic residue at P3 was more favourable for PfS1 inhibition.

Finally, to stabilize compound **8** toward putative peptidasic degradation and potentially increase its lifetime in the parasite egress assay, we introduced either a D-alanine (ala) (**14**), a *Cα*-methyl-leucine (Cml) (**15**) or a *Nα*-methyl-leucine (Nml) (**16**) (Figure 3). However, these changes led to a strong decrease in inhibitory potency and therefore lack of antiparasitic activity. Possible causes include steric hindrance due to the methyl group with the *D* configuration and/or disruption of the β-strand structure adopted by the inhibitor when binding to the enzyme. For compound **15**, the fully substituted α carbon stiffens the main chain, restricting to a non entirely canonical beta structure that could prevent tight fit in the groove. In the case of compound **16**, *N*-methylation of the P4-P3 peptide bond prevents the hydrogen bond with the Ser436 carbonyl group of the enzyme.

Table 1. PvS1 and PfS1 inhibitory potencies and percentage of merozoite egress inhibition at 100 (25) μM of α-ketoamide compounds **1-41** and of PM-IX/X reference inhibitor "49c".

Cpd	Structure[a]	IC_{50} (μM)[b]		Merozoite egress inhibition at 100 (25) μM[c] & IC_{50}
		$PvS1_{FL}$	$PfS1_{FL}$	
1	Ac-Ile-Thr-Ala-**AlaCO**-Asp-Glu(O-all)-NH_2	0.18 ± 0.02	1.95 ± 0.18	13%
P4 position				
2	Ac-**Aep**-Thr-Ala-**AlaCO**-Asp-Glu(O-all)-NH_2	0.46 ± 0.12	ND[d]	8%
3	Ac-**tBuGly**-Thr-Ala-**AlaCO**-Asp-Glu(O-all)-NH_2	0.21 ± 0.04	ND	4%
4	Ac-**tBuAla**-Thr-Ala-**AlaCO**-Asp-Glu(O-all)-NH_2	0.39 ± 0.07	ND	NI[e]
5	Ac-**Chg**-Thr-Ala-**AlaCO**-Asp-Glu(O-all)-NH_2	0.20 ± 0.06	1.95 ± 0.28	13%
6	Ac-**Cha**-Thr-Ala-**AlaCO**-Asp-Glu(O-all)-NH_2	4.08 ± 0.47	34.9 ± 8.9	NI
7	Ac-**Phg**-Thr-Ala-**AlaCO**-Asp-Glu(O-all)-NH_2	0.22 ± 0.07	ND	9%
8	Ac-**Cpg**-Thr-Ala-**AlaCO**-Asp-Glu(O-all)-NH_2	0.05 ± 0.01	0.57 ± 0.08	37%
P3 position				
9	Ac-Ile-**Trp**-Ala-**AlaCO**-Asp-Glu(O-all)-NH_2	0.24 ± 0.03	ND	5%
10	Ac-Ile-**Lys**-Ala-**AlaCO**-Asp-Glu(O-all)-NH_2	0.14 ± 0.03	ND	9%
11	Ac-Ile-**Dab(pyr)**-Ala-**AlaCO**-Asp-Glu(O-all)-NH_2	0.39 ± 0.08	ND	10%
12	Ac-**Cpg**-**Cpg**-Ala-**AlaCO**-Asp-Glu(O-all)-NH_2	0.08 ± 0.01	0.10 ± 0.01	46% (6%)
13	Ac-**Cpg**-**Tyr**-Ala-**AlaCO**-Asp-Glu(O-all)-	0.025 ±	0.15 ± 0.02	44%

	NH_2	0.014		
14	Ac-**Cpg**-**ala**-Ala-**AlaCO**-Asp-Glu(O-all)-NH_2	58,4 ± 2.8	ND	NI
15	Ac-**Cpg**-**Cml**-Ala-**AlaCO**-Asp-Glu(O-all)-NH_2	5.67 ± 0.47	ND	NI
16	Ac-**Cpg**-**Nml**-Ala-**AlaCO**-Asp-Glu(O-all)-NH_2	13.2 ± 3.2	ND	ND
P2 position				
17	Ac-Ile-Thr-**Gly**-**AlaCO**-Asp-Glu(O-all)-NH_2	1.28 ± 0.35	ND	ND
18	Ac-Ile-Thr-**Dha**-**AlaCO**-Asp-Glu(O-all)-NH_2	0.33 ± 0.04	ND	NI
19	Ac-Ile-Thr-**Abu**-**AlaCO**-Asp-Glu(O-all)-NH_2	0.35 ± 0.03	ND	ND
20	Ac-Ile-Thr-**Tfma**-**AlaCO**-Asp-Glu(O-all)-NH_2	3.60 ± 0.65	ND	ND
21	Ac-Ile-Thr-**Dap**-**AlaCO**-Asp-Glu(O-all)-NH_2	13.2 ± 1.2	ND	ND
22	Ac-**Cpg**-Thr-**Ser**-**AlaCO**-Asp-Glu(O-all)-NH_2	0.50 ± 0.17	ND	NI
23	Ac-**Cpg**-Thr-**Sar**-**AlaCO**-Asp-Glu(O-all)-NH_2	4.70 ± 0.90	ND	ND
24	Ac-**Cpg**-Thr-**Aib**-**AlaCO**-Asp-Glu(O-all)-NH_2	> 100	ND	NI
25	Ac-**Cpg**-Thr-**ala**-**AlaCO**-Asp-Glu(O-all)-NH_2	NI	ND	NI
P1 position				
26	Ac-Ile-Thr-Ala-**Dap(Ac)CO**-Asp-Glu(O-all)-NH_2	23.1 ± 0.7	ND	ND
27	Ac-**Cpg**-Thr-Ala-**Dap(Ac)CO**-Asp-Glu(O-all)-NH_2	2.39 ± 0.14	ND	NI
P1' position				
28	Ac-Ile-Thr-Ala-**AlaCO**-**Asn**-Glu(O-all)-NH_2	5.23 ± 1.80	ND	31%
29	Ac-Ile-Thr-Ala-**AlaCO**-**Glu**-Glu(O-all)-NH_2	2.90 ± 0.81	ND	ND
30	Ac-Ile-Thr-Ala-**AlaCO**-**Ser**-Glu(O-all)-	41.8 ± 5.4	ND	ND

	NH_2			
31	Ac-**Cpg**-Thr-Ala-**AlaCO**-**Ser**-Glu(O-all)-NH_2	10.9 ± 0.7	32.2 ± 1.0	11%
32	Ac-Ile-Thr-Ala-**AlaCO**-**Hse**-Glu(O-all)-NH_2	38.8 ± 14.6	ND	ND
33	Ac-**Cpg**-Thr-Ala-**AlaCO**-**βdiMeAsp**-Glu(O-all)-NH_2	0.18 ± 0.03	1.03 ± 0.15	3%
34	Ac-Ile-Thr-Ala-**AlaCO**-**Tza**-Glu(Oall)-NH_2	1.24 ± 0.08	24.4 ± 3.8	2%
35	Ac-**Cpg**-Thr-Ala-**AlaCO**-**Asp(O-all)**-Glu(O-all)-NH_2	1.32 ± 0.31	ND	17%
P2' position				
36	Ac-Ile-Thr-Ala-**AlaCO**-Asp-NH_2	0.17 ± 0.02	ND	3%
37	Ac-**Cpg**-Thr-Ala-**AlaCO**-Asp-NH_2	0.10 ± 0.03	0.55 ± 0.06	32%
38	Ac-Ile-Thr-Ala-**AlaCO**-**Tza**-NH_2	1.77 ± 0.05	ND	NI
39	Ac-**Cpg**-Thr-Ala-**AlaCO**-Asp-**Glu**-NH_2	0.030 ± 0.003	0.088 ± 0.006	NI
40	Ac-**Cpg**-Thr-Ala-**AlaCO**-Asp-**Cpg**-NH_2	0.012 ± 0.003	0.010 ± 0.003	100% (60%) *22.6 ± 5.7 μM*
41	Ac-**Cpg**-Thr-Ala-**AlaCO**-Asp-**Ile**-NH_2	0.014 ± 0.002	0.017 ± 0.005	99.8% (25%)
PM-IX/X reference inhibitor				
49c	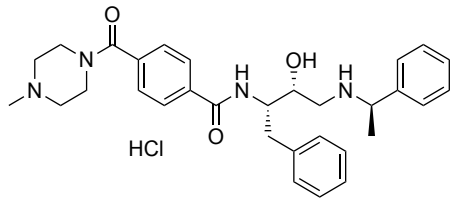	NI	ND	*1.1 nM*

[a]Abu, 2-Aminobutyryl; Aep, 2-Amino-3-ethyl-pentanoyl; all, allyl; Aib = α-aminoisobutyryl; tBuAla, tert-Butyl-Ala; tBuGly, tert-Butyl-Gly; Cha, Cyclohexylalanine; Chg, Cyclohexylglycine; Cml, Cα-MeLeu; Cpg, Cyclopentylglycine; Dab, 2,4-Diaminobutyryl; Dab(pyr), 2,4-Diaminobutyryl, N^4-pyrazinoyl; Dap, 2,3-Diaminopropionyl; Dha, dehydroalanine; Hse, Homoserine; Nml, *N*α-methyl-leucine; Phg, Phenylglycine; Sar, Sarcosine; Tfma, Trifluoromethylalanine; Tfmg, Trifluoromethylglycine; Tza, Tetrazole-Ala. [b]The activity of PvS1 and PfS1 was assessed using a FRET substrate (Dabsyl-KLVGADDVSLA-EDANS and Dabsyl-KLVSADNIDIS-EDANS for PvS1 and PfS1, respectively) [17] and followed by measuring the EDANS fluorescence (λ_{exc} at 360 nm and λ_{em} at 500 nm). All measurements were performed in triplicate. [c]Compound effect on *P. falciparum* merozoite egress from infected human erythrocytes was assessed as previously described [41]. All measurements were performed in triplicate. [d]ND, not determined. [e]NI, no inhibition.

2.2.1.3. Position P2. In SUB1 substrates, the P2 position is exclusively limited to the small residues Gly and Ala due to the restricted size of the S2 subsite (Figure 2). Substituting the Ala P2 residue of **1** with the smaller Gly (**17**) led to a 6-fold decrease in inhibitory potency towards PvS1 (Table 1). The introduction of a dehydroalanine (Dha, Figure 3) residue (**18**), of comparable size but inducing a local conformational change, was well tolerated. Side chain extension with additional methylene (i.e. 2-aminobutyryl (Abu), compound **19**) only slightly decreased the inhibitory efficacy. However, replacing Abu by its bulkier trifluorinated derivative trifluoromethylalanine (Tfma) in compound **20** led to a 10-fold decrease in activity. Adding an amino group to Ala (i.e. Dap, compound **21**) was even worse as the IC_{50} value of **21** was about 70-fold higher than that of **1**. In addition to a probably too large size, the potentially charged amino group of Dap may also not be favourable to interact in the S2 subsite. In fact, a polar but uncharged residue with comparable bulkiness to Dap (Ser in the **8** analogue **22**) was better tolerated with a 10-fold potency decrease compared to **8**. Finally, we replaced Ala of compound **8** by its *N*α-methylated isomer sarcosine (Sar) in compound **23**, its *C*α-methyl analogue α-aminoisobutyryl (Aib) in **24** and its *D* isomer in **25**. While compound **23** still inhibited PvS1 but with about more than 400-fold lower potency, no inhibition was observed for **24** and **25**. A comparable result was previously reported in the case of Aib [25]. Again, steric hindrance and/or β-strand stiffening and/or loss of an important hydrogen bond may be responsible of these very low potencies.

Overall, Ala remained the most favourable residue at this position in this series. Only compounds **22**, **24** and **25** were tested on the parasite culture and they were inactive (Table 1).

2.2.1.4. Position P1. In SUB1 substrates the P1 position is generally occupied by polar (Gln, Asn), charged (Glu, Asp) or small (Ala) residues (Figure 2) [28,44]. Whereas Gln is the most frequent, its α-ketoamide derivative is unstable and replacing the Ala side-chain by the Glu one slightly decreased the inhibitory potency [25]. Regarding Asp, a protected α-ketoacid derivative usable in solid phase synthesis has never been reported to our knowledge. Our attempts to prepare it following the synthetic pathway reported by J. W. Bode's laboratory [36] led to very low yields of the desired compound. Furthermore, peptide synthesis using this derivative was hampered by important secondary reactions, hence we could not obtain a sufficiently pure product.

In this context, we designed an unprecedented α-ketoamide derivative where the side chain was formed by N_{β}-Dap acetylation. Its side chain was isomeric to that of Gln and contained an amide group in different orientation and position, which should prevent any intramolecular cyclization. The P1 AlaCO residue of compounds **1** and **8** was therefore replaced by the Dap(Ac)CO analogue (Figure 3) to yield compounds **26** and **27**, respectively. Unfortunately, an important loss of inhibitory potency was observed and **27** was inactive in the cell assay (Table 1). Notably,

compound **27**, which contains a Cpg at P4, was about 10-fold more potent than **26**, confirming the high interest of this residue.

Further efforts are needed to optimize this position as the small methyl side-chain of AlaCO does not optimally fill the S1 subsite and the acquired knowledge about the αKA binding mode ([19] and the present study) should help the design of better matching P1 side chains. It has to be highlighted that, in this αKA series, the P1 residue is a β-amino acid and it is anchored by a covalent bond. Both facts might induce constraints on the side chain position and orientation and significantly change the side chain specificity in S1.

2.2.1.5. Position P1'. Asp and Ser are the most frequently observed residues at P1' position, while Asn and Glu are much less prevalent (Figure 2) [28,44]. In fact, replacing the Asp residue of compound **1** by Asn (**28**) or Glu (**29**) led to about 30- and 16-fold decrease in potency against PvS1, respectively, suggesting the necessity of a negatively charged group at this position and a limited space available in the S1' subsite. The importance of a negative charge was confirmed by substitution with a Ser residue as an even greater loss of activity (>200-fold) was measured for compound **30**. Again, the presence of a Cpg at P4 was favourable as **31** was about 4-fold more potent than **30** with Ile at this position. The adverse effect observed for Ser was not expected as it was shown that PfS1 was able to cleave equally well a SERA4-derived decapeptidic substrate and the analogue in which the P1' Asp residue was substituted with Ser [18]. This significant difference regarding the impact of the P1' residue questions the relevance of using the *in vivo P. berghei* rodent malaria model since the PbS1 orthologue has a strong preference for Ser at position P1' and poorly cleaves substrates with Asp [18]. We also introduced the Ser homologue homoserine (Hse) (i.e. **32**), but without change in potency compared to **30**. Replacing Asp of compound **8** by its bulkier and more hydrophobic β-dimethyl analogue (compound **33**) led to about 3- and 2-fold lower inhibition of PvS1 and PfS1, respectively, confirming the limited volume of the S1' subsite. In addition, this compound was only poorly active in the parasite egress assay. Considering that the negative charge of Asp is very probably detrimental to membrane crossing while being important for efficient binding, we substituted the carboxylic group with its 1*H*-tetrazole bioisostere (Figure 3) [46,47]. Unfortunately, although the Tza-containing compound **34** was a better PvS1 inhibitor than the corresponding Asn (**28**) and Glu (**29**) analogues, it was approximately 7-fold less potent than **1** and inactive in the cell assay. This result might be due to the larger size of the tetrazole moiety compared to the carboxylic group. Finally, we prepared compound **35** containing an allyl-protected Asp P1' residue to remove the negative charge and favour cell penetration, hopping intracellular ester hydrolysis. As expected, a strong decrease (200-fold) in inhibitory potency toward PvS1 was observed, while modest (17% inhibition at 100 μM) antiparasitic activity was

measured, partially but insufficiently validating our design strategy. Overall, the present results suggested that an Asp at P1' position is mandatory to preserve significant potency against Pv/PfS1. Other smaller carboxylic isosteres should be evaluated, which requires the synthesis of the appropriate Fmoc-protected amino acids.

2.2.1.6. Position P2'. To assess the possible role of the P2' Glu(O-all) residue, we prepared compounds **36**, **37** and **38**, which are analogues of **1**, **8** and **34**, respectively, devoid of this residue. They showed similar IC_{50} values as their parent analogues against PvS1 enzymes, indicating that the P2' side-chain does not contribute to binding. This result is consistent with the X-ray structure of the $PvS1_{CD}$/**1** complex, in which the side chain of the P2' residue could not be resolved suggesting an important flexibility due to the absence of interaction with $PvS1_{CD}$ catalytic groove [19]. However, their antiparasitic activity was decreased. Deprotecting the P2' side chain of **8** (i.e. compound **39**) slightly increased the inhibitory potency toward PvS1 (IC_{50} value 0.03 vs 0.05 μM for **8**). Interestingly, a stronger improvement (about 6-fold) was observed against PfS1 (IC_{50} value of 0.088 μM) but the antiparasitic activity was fully abolished. This result is presumably due to the presence of a second negatively charged residue, decreasing the ability to cross cell membranes. Finally, we substituted the Glu(O-all) moiety by more hydrophobic residues as Cpg and Ile in compounds **40** and **41**, respectively. Unexpectedly, this change led to an increase inhibitory potency against both Pv- and PfS1. In particular, a 50-fold increase was observed for PfS1 in the case of compound **40** compared to **8** (IC_{50} values 0.010 vs 0.57 μM). In fact, compound **40** is the best inhibitor of both Pv- and PfS1 in this study, with close IC_{50} values. In addition, it displayed the highest antiparasitic activity, for which an IC_{50} value of 22.6 ± 5.7 μM was measured (Figure S1). Apart its higher PfS1 inhibitory potency, this result may also be due to the higher hydrophobicity of the compound compared to most other analogues, a property expected to be favourable for cell penetration. The calculation of clogP for selected compounds (**1**, **8**, **12**, **40**, **41**) confirmed their expected relative hydrophobicities (Table S3). It is interesting to note that the presence of a Cpg residue at several positions, P4 (**8**), P3 (**12**) and P2' (**40**) was favorable to SUB1 inhibition and antiparasitic activity.

To support that the observed antiparasitic activity was related to SUB1 inhibition, we determined if compound **40** had an effect during the trophogony, the first part of the intra-erythrocytic cycle of *Plasmodium* sp., where active SUB1 is known to be absent. Compound **40** was incubated in a synchronous parasite culture containing young rings, corresponding to parasites prepared 0-3 hours post-invasion into human erythrocytes, and cultivated for 28 h. After compound removal and further culture for 38 h, 6% and 0% growth inhibition, not related to SUB1, were measured in the presence of 100 and 25 μM compound **40**, respectively. A selectivity index (SI = 1 - (% trophogony

inhibition/% T0-T8 merozoite egress assay inhibition) of 0.94 was calculated at 100 µM (1.0 was calculated at 25 µM), suggesting that the antiparasitic activity of **40** was indeed specific to the second part of the erythrocytic life cycle up to the egress and invasion steps where SUB1 is involved.

2.2.2 Thermal stability, dissociation kinetics, enzyme selectivity analysis and stability in human serum

Differential scanning fluorimetry (DSF) was employed to evaluate the ΔTm values for $PvS1_{CD}$ in the presence of various inhibitors, including compounds **2**, **3**, **5**, **6**, **7**, **8**, **17**, and **40** (Figure S2). Our analysis revealed a positive correlation between inhibitory potencies (indicated by IC_{50} values) and ΔTm values. It is noteworthy that binding with the most potent inhibitors **8** (14.3 ± 0.1 °C) and **40** (12.7 ± 0.3 °C) yielded the highest ΔTm values and thus the greatest thermal stabilities. In contrast, the complex with the least potent inhibitor **6** exhibited the lowest ΔTm value (6.8 ± 0.2 °C).

The dissociation kinetics of compounds **1**, **5**, **8**, **34** and **37** on $PvS1_{CD}$ were examined using a jump dilution assay. Complex formation was facilitated through overnight incubation, followed by the initiation of dissociation by dilution in a fluorescent substrate solution. Enzymatic activity recovery was monitored over a two-hour period and the experimental data were fitted to the function $F(t) = V_s \times t + (V_i - V_s) \times [1 - \exp(k_{obs} \times t)]/k_{obs}$ to determine the dissociation rate constant ($k_{obs} \approx k_{off}$). Compound **8** displayed the most favourable dissociation kinetics, with a k_{off} of 0.023 min^{-1} and a bound half-life ($t_{1/2off}$) of 30 minutes (Table 2). In comparison, the shortened analogue **37** had a k_{off} value of 0.034 min^{-1} and a $t_{1/2off}$ of 20 minutes, while the reference compound **1** had a k_{off} value of 0.074 min^{-1} and a $t_{1/2off}$ of 10 minutes. Interestingly, the jump-dilution assay failed to reveal k_{off} results for compounds **5** and **34**, possibly due to their high release rates.

Table 2. Inhibitor binding kinetics and half-lives on $PvS1_{CD}$.[a]

Cpd	IC_{50} (µM) on $PvS1_{CDb}$	k_{off}, min^{-1}	Bound half-life ($t_{1/2off}$), min
1	0.10 ± 0.04	0.074	10
5	0.15 ± 0.05	ND	NA
8	0.070 ± 0.003	0.023	30
34	2.22 ± 0.44	ND	NA
37	0.150 ± 0.005	0.034	20

[a]ND and NA stand for not determined and not applicable, respectively. [b]IC_{50} values from Table S2.

Our findings suggest that compounds **1**, **8**, and **37** behave as slow tight-binding inhibitors, and that the increased *in vitro* potency and biological effect of compound **8** may be attributed to its enhanced capacity for slow reversibility.

Furthermore, the selectivity of compound **8** was evaluated against three mammalian peptidases, trypsin, chymotrypsin and elastase. As anticipated, no significant inhibition of trypsin and chymotrypsin was observed. In contrast, significant inhibition of elastase was detected (Figure S3), which was expected due to the elastase preference for small uncharged residues at the P1 position. Nevertheless, the IC_{50} value measured against elastase (i.e. 36 µM) was 720- and 63-fold higher than for $PvS1_{FL}$ and $PfS1_{FL}$, respectively, indicating a high selectivity of **8** toward the plasmodial enzymes. Similar results were obtained for a peptide boronate SUB1 inhibitor, while it displayed a lower IC_{50} value of 0.82 µM against elastase [29].

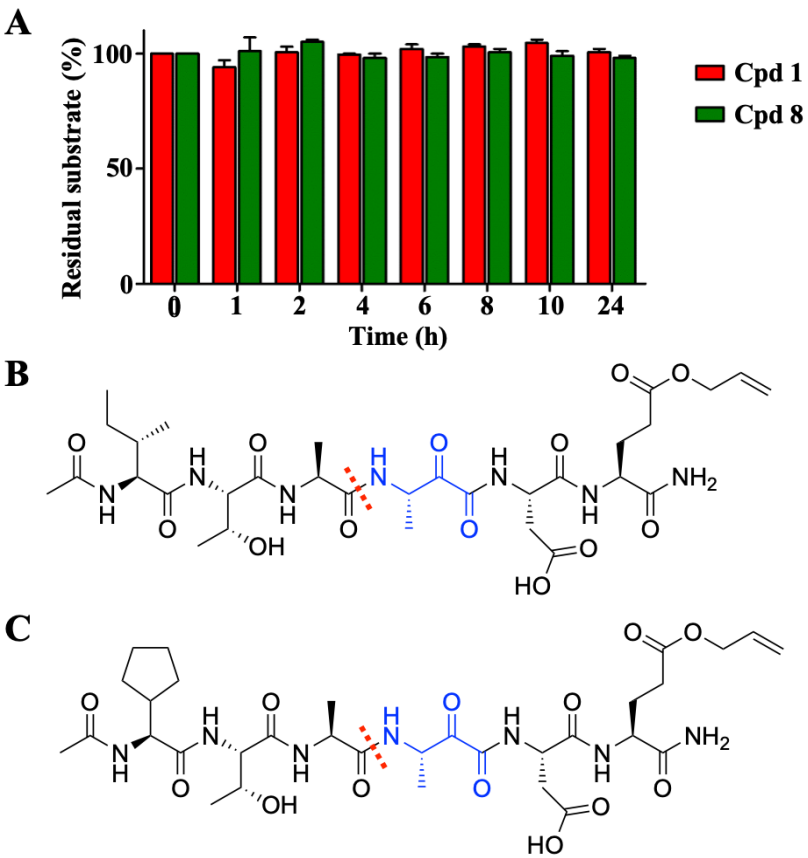

Figure 4. (A) Comparison of the *in vitro* metabolic stability of SUB1 inhibitors **1** and **8** in human serum. Results are presented as the means ± SEMs of two independent LC-MS experiments (N = 2). In order to show the absence of significant differences in the concentration of intact substrate at each time interval, a two-way ANOVA with Bonferroni's post-tests was done. Bonds potentially cleaved in compounds **1** (B) and **8** (C) are marked with a red dashed line.

Finally, the stability of compounds **1** and **8** was assessed in human serum at 37 °C, which contains potentially degrading proteases (Figure 4). Samples were taken at different time intervals (0-24 h)

of incubation and analysed using LC-MS. Both analogues exhibited very high stability toward enzymatic degradation with around 95% of each compound still being intact after 24 h (Figure 4A). Analysis of the metabolites by LC-MS, predicted by their theoretical masses, showed that only one amide bond, between P2 and P1 residues, was hardly hydrolysed (Figure 4B and 4C and Table S4, Figures S4 and S5). Overall, this result suggests that the compounds are fully stable during the *in vitro* parasite growth assay.

Taken together, these findings indicate that compound **8** is a potent inhibitor of PvS1, exhibiting slow tight-binding properties, high selectivity toward tested enzymes and high stability in biological media such as serum.

2.3. Structural studies

We have successfully determined the crystal structures of $PvS1_{CD}$ (residues 277-617) in complex with compounds **3** (tBuGly at P4), **7** (Phg at P4), and **8** (Cpg at P4) following previously established conditions [19] (Table S5). Consistent with what has been observed for compound **1** (pdb code 8COY), all three complexes crystallized in the same space group (P1). The binding pocket structures in complexes with compounds **3** and **7** are illustrated in Figures 5A and 5B, respectively. A close inspection of Figure S6A reveals that the PvS1-bound conformation of these compounds are nearly identical to that of compound **1** [19]. Comprehensive details regarding the crystallographic complexes of compounds **3** and **7** can be found in Supplementary Material.

The structure of $PvS1_{CD}$ in complex with compound **8** was solved at 1.5 Å resolution (Figure 5C). As expected, a molecule of **8** was found to be bound to both of the two PvS1 polypeptide chains (i.e. chains A and B) present within the asymmetric unit. Superposition of chains A and B revealed that both chains are nearly identical (RMSD of 0.28 Å for all Cα atoms aligned). The complex showed clear electron density for the $PvS1_{CD}$ active site of both polypeptides present in the asymmetric unit (Figure S7).

Superposition of binding pockets of chains A and B (residues Asp316, Tyr371, His372, Leu405, Lys409, Leu410, Gly411, Arg412, Leu413, Met416, Ser434, Phe435, Ser436, Phe437, Asp438, Ser461, Ser463, Asn464, Leu545, Asn546, Gly547, Thr548, Ser549, and Met550) revealed they are identical (RMSD of 0.06 Å). Electron density was equally clear around compound **8**, which was easily modelled (Figure S7C) from the acetyl group to P1', with P2' being only partially visible, possibly due to a lack of contact with the protein leading to an increased flexibility, as previously observed for compound **1** ([19]; pdb code 8COY). The three Ramachandran outliers (D316, catalytic activator; Y371, P1'; S463, P1; 0.9%) observed for the $PvS1_{CD}$/**8** complex structure are well-defined in density, and all of them are part of the substrate-binding site, where they interact with the bound inhibitor.

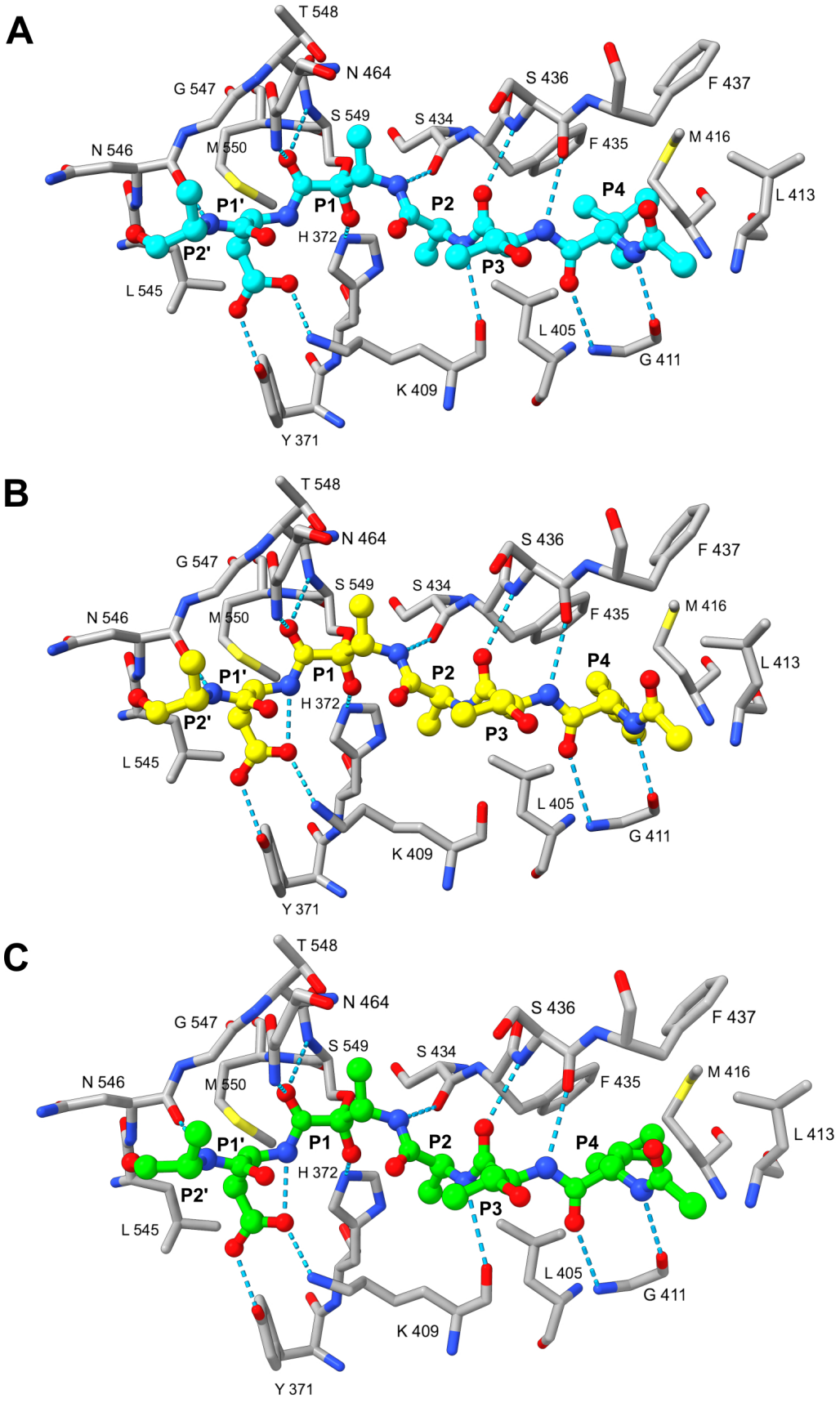

Figure 5. Details of $PvS1_{CD}$ residues (shown in grey) involved in the interaction with compounds **3**, **7** and **8** (A, B and C, respectively). Hydrogen bonds are depicted as blue doted lines. P4-P2' positions of all three compounds are indicated.

Comparative structural analysis of the complex crystal structures with compounds **1** and **8** indicates that the overall structures are nearly identical, with an overall RMSD of 0.30 Å, and of 0.14 Å for the peptide binding pocket (Figure S8). Compound **8** also superimposed very well with its analogue **1** when bound to $PvS1_{CD}$ (Figure S6B). Careful observation of the superposed structures revealed that most of the interactions between $PvS1_{CD}$ and the ligands are shared. As observed for compound **1**, the catalytic Ser549 residue is engaged in a covalent bond with the carbon atom of the α-keto group of **8**, trapping SUB1 in a transition state-like configuration. The hydrogen bonds with Tyr371, Lys409, His372, Ser549, Ser434, Gly411, Ser436, Asn464, and Asn546 are equally conserved (Figure 5C and S9C). The pattern of predicted hydrophobic interactions is mostly conserved (Tyr371, His372, Leu405, Lys409, Leu410, Gly411, Leu413, Met416, Ser434, Phe435, Ser436, Phe437, Asn464, Leu545, Asn546, Gly547, Thr548, and Ser549, Figure S9C). Small differences include the lack of compound **1** interaction with Met550 and a new interaction with Thr493 for the analogue **8**. The pattern of hydrophobic interactions slightly differs with respect to interactions with the P4 positions of compounds **1** (Ile) and **8** (Cpg). While the Cpg side chain of **8** was observed to interact with Leu405, Leu413, Met416, Phe435, and Ser436, the Ile side chain of **1** was found to interact with Leu405, Gly411, Leu413, and Met416. This difference could potentially contribute to the higher potency observed for compound **8** over **1**.

3. Conclusions

The pseudopeptide αKA **1** corresponds to the P4-P2' segment derived from the SUB1-dependent maturation site of PfSERA4, where the P1 Gln residue has been replaced by Ala. It inhibited Pv- and PfS1's with IC_{50} values in the low submicromolar and micromolar ranges, respectively, and modestly inhibited the egress of *P. falciparum* merozoites in culture (13% inhibition at 100 μM). Here, we described our first efforts to optimize the reference inhibitor **1** by studying its structure-activity relationships. By substituting the residues driving SUB1 recognition (i.e. P4, P2, P1, P1' residues) with structurally similar amino acids, we identified up to five-fold more potent Pv/PfS1 inhibitors. In particular, whereas no change at P2, P1 and P1' positions was favourable, substitution at P4 afforded the largest improvement. Indeed, a Cpg at this position (compound **8**) resulted in the most important effect. This behaviour was also observed in several other analogues that were synthesized in the two versions, Ile or Cpg at P4 (i.e. **27** vs **26**, **31** vs **33**). A similar result was reported independently for PfS1 boronate inhibitors [29]. The reason why the Cpg residue was so favourable could be analyzed thanks to the resolution of the crystallographic structure of the complex PvS1/**8**. Yet, structures showed similar binding mode as for compounds **1** [19], **3**, **7** and **8**

and thus did not reveal any striking feature of Cpg. Nonetheless, **8** appeared as an optimum in terms of size in the series Ile/Cpg/Chg, with a puckered trapezoidal shape satisfactorily fitting the S4 subsite. It is also hypothesized that Cpg displays a higher rigidity compared to other tested P4 residues thanks to its cycle, which could lead to reduced entropic contribution favoring unbounded state. Importantly, the improved enzyme inhibition by **8** vs **1** was associated with better antiparasitic activity. In addition, compound **8** showed high selectivity for SUB1 over three mammalian serine peptidases and was found stable when incubated in human serum for 24 h, making this compound a promising basis for further optimization.

Unexpectedly, modifications at the P3 and P2' positions, which are not directly involved in SUB1 binding, could led to improved inhibition, particularly against PfS1 (see compounds **12**, **13**, **40** and **41**). This improvement might be related to an increase in hydrophobicity. It is noteworthy that the IC_{50} ratio between PvS1 and PfS1 varied from 10 for compound **8** to about 1 for compounds **12**, **40** and **41** with a single change at the P3 or P2' position. Interestingly, the higher PfS1 inhibitory potency was accompanied by a better antiparasitic activity.

In fact, the variable relative efficiency of a given compound against Pv- and PfS1 (e.g. PfS1/PvS1 IC_{50} ratios of 10 (**1**, **8**), 5 (**33**), 3 (**39**), 1 (**12**, **40**)) is not clearly understood as the active sites of the two enzymes are highly conserved and they share very close substrate profiles [17,18,20]. These differences may be attributed to variable reversibility rates of the covalent enzyme/inhibitor complexes.

In addition to the magnitude of SUB1 inhibition, the ability to penetrate cells should also affect the efficacy of compounds in blocking merozoite egress. Indeed, the compounds have to cross two membranes (i.e. the erythrocytic membrane and that of the parasitophorous vacuole) to reach active SUB1. As cell membrane penetration is at least partly dependent on compound hydrophobicity, we likewise observed that, with comparable IC_{50} values, the more hydrophobic the compounds, the higher potency in the *in vitro* parasite assay. For instance, the fully unprotected compound **39** (two negative charges) was inactive on the parasite, although it was a 6-fold better PfS1 inhibitor than its allyl-protected analogue **8** (one negative charge). As said above, higher hydrophobicity could also led to stronger PfS1 inhibition, associated with an increase in antiparasitic activity. In particular, compound **40** was the most potent inhibitor of both Pv- and PfS1 (IC_{50} values of about 10 nM) and also displayed the higher antiparasitic activity in this series with an IC_{50} of 22.6 ± 5.7 μM on merozoite egress assay and a selectivity index of 0.94 supporting that parasite growth inhibition was related to SUB1 inhibition.

The wide substitutions at individual positions and their consequences regarding the inhibition of SUB1, together with the structural data obtained through the X-rays resolution of four

SUB1/inhibitor complexes provide important informations for the rational design of the next generation of SUB1-specific inhibitors. Further efforts are indeed needed to improve the anti-parasitic potency of SUB1 inhibitors, with increased affinity and cell penetration properties. Structural driven new syntheses and the modulation of global properties of optimized inhibitors, including by exploring *N*-terminal modifications, could finally define an anti-SUB1 lead compound.

4. Experiment section

4.1.Materials

Fmoc-protected amino acids, HATU, BOP and Fmoc-protected Rink amide polystyrene resin were purchased from IrisBiotech or Novabiochem. Other reagents and solvents were purchased from Acros Organics, Alfa Aesar, Carlo Erba or Sigma-Aldrich and used without further purification. Solvents used for HPLC and LC-MS were of HPLC grade.

4.2. Synthesis of amino acid derivatives

The synthesis of special Fmoc-protected amino acid derivatives is described in the Supplementary Material part.

4.3. Peptide synthesis

Peptide chain assembly was stepwise and manually carried out in a plastic syringe equipped with frit following the Fmoc/tBu strategy. All final compounds were purified by preparative reverse-phase HPLC (RP-HPLC) and the purity was assessed by analytical RP-HPLC and LC-MS analyses.

4.3.1. Manual synthesis

The Fmoc-protected Rink amide resin (100-200 mesh, 0.5-0.6 mmol/g) was swelled for 30 min in DMF. After filtration, the Fmoc group was removed through two consecutive treatments with piperidine/DMF (20/80, v/v) for 10 and 25 min. Coupling of Fmoc-protected amino acids (3 equiv. according to the resin loading) was carried out in DMF or NMP in the presence of HATU (3 equiv.) and DIEA (4 equiv.) for 2 h. After each step, the resin was washed with DMF, MeOH and DCM. Monitoring of the deprotection and coupling steps was performed using the 2,4,6-trinitrobenzenesulfonic acid test (TNBS) [48]. A second coupling was performed when necessary.

The coupling of the Fmoc-protected norstatine and protected α-ketoacid building blocks was performed with two equivalents of the amino acid in the presence of HATU or BOP (2 equiv.) and DIEA (3 equiv.) for 5 h.

To prepare compound **11** (Table 1), which possesses a *Nγ*-pyrazinoyl-Dab at the P3 position, we introduced Fmoc-Dab(Mtt)-OH during solid phase synthesis. After complete peptide assembly, Mtt was selectively removed by six treatments with the mixture DCM/TFE/AcOH/TIS (7:2:1:0.25, 10

mL/g of resin; TFE, trifluoroethanol; TIS, triisopropylsilane) and the free amine was coupled with pyrazinoic acid in standard conditions.

At intermediate steps the on-resin growing peptide was controlled by cleaving it from 2-3 mg of resin with 500 μL trifluoroacetic acid (TFA) and analysing the isolated sample by RP-HPLC and LC-MS as described in the Supplementary Material part.

4.3.2. N-terminal acetylation

Acetic acid was coupled to the *N*-terminal amine in the same manner as Fmoc-amino acids.

4.3.3. Formation of the α-ketoamide group from norstatine-like residues

After peptide assembly, the secondary alcohol function of the norstatine derivatives was oxidized using Dess-Martin Periodinane (DMP). The resin was swelled in a mixture of dry DMF/DCM (1:1) and 3 equiv. of DMP were added. After overnight stirring at rt and in the dark, the resin was filtered and washed with DMF and DCM. The treatment was repeated.

4.3.4. Cleavage of peptide resins

The peptides assembled with norstatine-like residues were simultaneously cleaved from the resin and deprotected by a 2h treatment with a mixture of TFA, TIS and water (95:2.5:2.5, 10 mL/g). After filtration, the TFA was concentrated in vacuo. Compounds were precipitated by addition of diethyl ether and recovered after centrifugation. The pellet was washed twice with diethyl ether. When the alanine-derived protected α-ketoacid was used, the cleavage was performed in two steps: (i) 2h treatment with the mixture TFA/TIS/H_2O/DODT (91/3/3/3) (DODT, 3,6-dioxa-1,8-octanedithiol) followed by filtration, precipitation in diethyl ether and centrifugation. (ii) The pellet was then treated with TFA/DODT/H_2O for 2h and the fully deprotected compounds were recovered as described above. All compounds were purified by RP-HPLC as described in Supplementary Material part and yields, RP-HPLC and LC-MS data are presented in Table S1.

4.4. Biological evaluation

4.4.1. Production of P. vivax *and* P. falciparum *SUB1 recombinant enzymes*

Full-length recombinant $PvS1_{FL}$ and $PfS1_{FL}$ (Genbank JX491486 and FJ536585, respectively) were prepared as previously described [17,20]. Briefly, Sf9 cells were infected with recombinant baculovirus, and the culture medium containing either $PvS1_{FL}$ or $PfS1_{FL}$ was clarified by centrifugation and concentrated/diafiltrated against IMAC loading buffer. Purified fractions were then tested for activity using a FRET-based assay and pure active fractions were pooled, concentrated, and stored at -20°C [17].

The recombinant prodomain-free catalytic form of PvS1 ($PvS1_{CD}$) was prepared as previously described for both IC_{50} measurements and co-crystallization trials [19]. Briefly, selected *Drosophila* S2 cells stably transfected with the $PvS1_{FL\text{-}ng}$ construct (GenBank™ MZ344794) encoding for $PvS1_{FL}$ mutated at positions N356S, N427S and N440S to prevent unwanted *N*-glycosylation, were cultivated in Insect-XPRESS medium (Lonza) and $PvS1_{FL\text{-}ng}$ expression was induced by adding 5 µM of $CdCl_2$ to transfected *Drosophila* S2 cells. $PvS1_{FL\text{-}ng}$ was purified from concentrated/diafiltrated culture supernatant by chromatography on a 5-mL TALON metal affinity resin (Clontech). $PvS1_{CD}$ was obtained following incubation of $PvS1_{FL\text{-}ng}$ in a dissociation buffer (50 mM Tris, 2 M $MgCl_2$, pH 8) allowing the dissociation of $PvS1_{FL\text{-}ng}$ prodomain and subsequent trypsin digestion for 2.5 h at 25 °C. Active pure fractions containing $PvS1_{CD}$ obtained after size-fractionation onto a HiLoad 16/60 Superdex 75 column equilibrated with 20 mM Tris, 50 mM $CaCl_2$ (pH 8) were pooled and stored at -20 °C with 10% v/v of glycerol for activity assays or with 2% v/v PEG8000 for crystallization studies.

4.4.2. Enzymatic test and determination of inhibitory potencies

The activity of PvS1 and PfS1 was assessed using a FRET substrate on a 384-wells plate as previously described [17]. Briefly, compounds at 10 different concentrations were incubated with $PvS1_{FL\ or\ CD}$ or $PfS1_{FL}$ at 37 °C for 15 min in 25 mM $CaCl_2$, 0.1% Chaps, pH 7.5. The reaction was initiated by adding the FRET substrate (20 µM) (Dabsyl-KLVGADDVSLA-EDANS and Dabsyl-KLVSADNIDIS-EDANS for PvS1 and PfS1, respectively) and followed by measuring the EDANS fluorescence (excitation at 360 nm and emission at 500 nm) every 2 min under shaking over 1h using a Tecan Infinite M1000 spectrofluorimeter. IC_{50} values were calculated using GraphPad PRISM software. All measurements were performed in triplicate.

4.4.3. Thermal shift assay of $PvS1_{CD}$ in the presence of inhibitors

To determine the melting temperature (Tm) of $PvS1_{CD}$ by differential scanning fluorimetry (DSF) in the presence and absence of inhibitors, 2.5 µg of $PvS1_{CD}$ in 20 mM Tris pH 8.0, 150 mM NaCl, 25 mM $CaCl_2$, 250 mM $MgSO_4$ and 1 mM dithiothreitol supplemented with either 1 mM compound or 5% DMSO was dispensed into 96-well PCR plates (25 µL per well). A 50X solution of Sypro Orange (Invitrogen) was added to each well (2.5 µL per well), and the plate was heated from 25 to 95°C in 1 °C steps of 1 minute each using a CFX96 Touch™ Real-Time PCR Detection System (BioRad). Fluorescence increase resulting from the binding of Sypro Orange to the exposed hydrophobic regions of the unfolding protein was monitored using the FRET filter. The melting temperature (Tm) was defined as the midpoint of the protein unfolding transition.

4.4.4 Jump dilution assay for dissociation kinetics evaluation

The jump dilution assay was adapted from [49]. Initially, to quantify the concentration of active enzyme molecules ([E]t) capable of binding the inhibitors, we adopted a method outlined in the literature [50]. Briefly, an enzymatic assay with the chosen compounds was conducted using the FRET method mentioned above, adjusting the highest concentration in the assay to be 100 times the previously calculated IC_{50}. The initial velocities were then plotted against inhibitor concentrations and fitted to the Morrison equation to obtain the [E]t values [51]. Subsequently, enzyme:complex mixtures were prepared at equal concentrations, taking into account the active enzyme concentration [E]t. The mixtures contained 2.8 µM active $PvS1_{CD}$, 2.8 µM compound, 25 mM $CaCl_2$, 0.5 % Chaps, 20 mM Tris pH 7.5, and 10% DMSO (to ensure solubility of the compound) in a 30 µM final volume. Non-inhibited control (no compound) and negative control (no enzyme) reactions were performed in parallel. The components were mixed in a 96-well microtiter plate, which was then sealed and incubated overnight at room temperature. The next morning, the enzyme:inhibitor interaction was assumed to have reached binding equilibrium. A two-step 100-fold dilution was carried out to induce the breakdown of the complex. A 20-fold dilution was performed in 25 mM $CaCl_2$, 0.5 % Chaps, 20 mM Tris pH 7.5, and 10% DMSO, followed by a 5-fold dilution in a solution containing the same components plus 20 µM of the FRET substrate (Dabsyl-KLVGADDVSLA-EDANS). The final dilution was transferred to a black 384-well flat-bottom plate (18 µL per well), spun down, and fluorescence measurements were initiated. The plate reader was set up for a 2-hour measurement with readings every minute at 360/500 +/- 10 nm and 25 °C. The data plots of fluorescence as a function of time were analyzed using nonlinear regression and fit to the following equation: $F(t) = V_s \times t + (V_i - V_s) \times [1 - \exp(k_{obs} \times t)]/k_{obs}$. In these experiments, k_{obs} is expected to be within 20% of the k_{off} value [49]. The bound half-life ($t_{1/2off}$) was determined from the k_{off} value using the equation: $t_{1/2off} = 0.693/k_{off}$.

4.4.5. Inhibition assays for mammalian serine peptidases: trypsin, chymotrypsin, elastase

Inhibition assays for mammalian serine peptidases were performed based on the method described by Lainé et al. [52]. Trypsin (from porcine pancreas; Sigma-Aldrich T4799), chymotrypsin (from bovine pancreas; Sigma-Aldrich C4129), and elastase (from porcine pancreas; Sigma-Aldrich E1250) activity measurements were based on the cleavage of the substrates *Nα*-benzoyl-L-arginine-*p*-nitroanilide hydrochloride (Sigma-Aldrich B3133), *Nα*-succinyl-Ala-Ala-Pro-Phe-*p*-nitroanilide (Sigma-Aldrich S7388), and *Nα*-succinyl-Ala-Ala-Ala-*p*-nitroanilide (Sigma-Aldrich S4760), respectively. A stock solution of 1 mg/mL for each peptidase was prepared in 100 mM Tris-HCl, pH 8.0, and 20 mM $CaCl_2$. The substrates were prepared as 200 mM stock solutions in DMSO. Inhibition measurements were performed in 96-well clear, flat-bottom plates. For each peptidase, 5 µg/mL of trypsin, 0.5 µg/mL of chymotrypsin, or 5 µg/mL of elastase in 98 µL assay buffer (100 mM Tris-HCl, pH 8.0, and 20 mM $CaCl_2$) was mixed with 2 µL of compound at 10 mM and

incubated for 15 min before the addition of 100 µL of substrate pre-diluted in assay buffer to yield a final concentration of 1 mM. Phenylmethylsulfonyl fluoride (PMSF) at a final concentration of 2 mM was used as an inhibition control, while pure DMSO was used as a non-inhibition control. For all three enzymes, activity detection was performed by monitoring the absorbance at 405 nm for one hour. To estimate the inhibitory potential of compound **8** on elastase, the assay was repeated at a range of 10 concentrations of inhibitor starting at 600 µM. The slope values of the linear part of the activity curves were obtained with the Magellan software, and IC_{50} values were calculated using the GraphPad Prism software. All measurements were performed in triplicate.

4.4.6. Evaluation of SUB1 inhibitors on P. falciparum *merozoite egress from infected human erythrocytes and selectivity index determination*

Parasites were cultured as previously described [17] in RPMI 1640 medium containing L-glutamine, 25 mM HEPES (Invitrogen) supplemented with 2.5% Albumax II (Gibco), with a hematocrit (human red blood cells) of 5%, 100 µM hypoxanthine (C.C.pro, Germany), 25 µg/mL gentamycin (SigmaAldrich) at 37 °C in a 5% O_2, 5% CO_2, and 90% N_2 atmosphere. To obtain human red blood cells, peripheral blood samples were collected from healthy volunteers through the ICAReB platform (Clinical Investigation & Access to Research Bioresources) from the Center for Translational Science, Institut Pasteur [53]. All participants received an oral and written information about the research and gave written informed consent in the frame of the healthy volunteers Diagmicoll cohort (Clinical trials NCT 03912246) and CoSImmGEn cohort (Clinical trials NCT 03925272), after approval of the Ethics Committee of Ile-de-France (2009 April 30th and 2011 jan 18th, respectively).

Compound effect on *P. falciparum* merozoite egress from infected human erythrocytes was assessed using the method previously described by Bouillon et al. [41] with minor adjustments (T0-T8 assay). Briefly, *P. falciparum* cultures were synchronized using successive sorbitol treatments, and schizonts were isolated through plasmion purification. The synchronized cultures, mainly composed of late schizonts, were adjusted to 2% hematocrit and 1% parasitemia and exposed to compounds at the desired concentrations. After an 8-hour incubation at 37°C, the samples were fixed with a 0.04% glutaraldehyde solution in phosphate-buffered saline (PBS), permeabilized with 0.25% Triton X-100, and treated with RNAse (0.05 mg/mL, Sigma-Aldrich) before staining with YOYO-1 DNA binding dye (400 nM final concentration, Invitrogen). The flow data were acquired using MacsQuant flow cytometer with 100,000 events per sample and analyzed using FlowJo software to determine the parasitemia of ring stage parasites after egress and invasion. The inhibition percentage was calculated comparing with the parasitemia obtained with the control DMSO. Compound **40** was tested on 16 different concentrations from 180 to 0.8 µM to determine a

precise IC_{50} in the T0-T8 assay. The experiment has been done in triplicate and IC_{50} value was calculated using GraphPad PRISM software.

SUB1 being specific for mature *Plasmodium* schizonts and involved in the merozoite egress, the eventual off-target effect of compound **40** has been evaluated on *P.falciparum* trophogony, namely the phase during which young post-invasion parasites, until early schizogony, when the parasites start dividing in daugther merozoites. A synchronous parasite culture (2% hematocrit and 1% parasitemia) of young trophozoites (called "rings") aged of 0-3 hours post-invasion into red blood cells was exposed to 100 and 25 µM compound **40** or an equivalent amount of DMSO (1% and 0.25% final, respectively) during 28h. The culture medium was then removed, infected red blood cells were washed and put back in culture without compound for 38h, allowing the completion of the intra-erythrocytic cycle and a merozoite egress/invasion event to occur before the samples were fixed and parasitemia were determined as described above. Comparing with the parasitemia obtained with the DMSO control, a percentage of parasite growth inhibition not related to SUB1 was calculated. The selectivity index (SI) corresponds to : SI = 1 - (% trophogony inhibition/% T0-T8 assay inhibition), % T0-T8 assay inhibition being 100% and 60% at 100 and 25 µM compound **40**, respectively. A SI close to 1 gives an indication on SUB1 target specificity.

4.4.7. Stability assay in human serum

A degradation assay was described previously [54] and full details are given in the Supplementary Materials part. Briefly, pooled human serum was preincubated in Eppendorf ThermoMixer® Comfort (Hamburg, Germany) for 20 min at 37 °C (350 rpm), followed by addition of 20 µL of aqueous peptide stock solution (0.6 mM final concentration in serum) and further incubation. At selected time intervals, samples of 50 µL were collected and mixed with 200 µL of MeCN:H_2O:formic acid mixture (89:10:1, v:v:v) to precipitate serum proteins. The suspension was vortexed and centrifuged (10 min, 4 °C, 11 000 g). 100 µL of supernatant were collected and lyophilized. The samples were reconstituted in 1 mL of 10 mM ammonium formate with 0.1% formic acid in water, vortexed and subjected to LC-SWATH-MS (SWATH-MS = Sequential Window Acquisition of All Theorical Mass Spectra). Quantification was done by measuring the intensity of extracted ion chromatograms (XIC) obtained by MS analysis: for both **1** and **8** we chose the fragment ion 573.2492 *m/z* and its intensity was plotted as a function of time. The electrospray ionization (ESI) was operated in positive mode.

For identification of potential degradation products and quantification (degradation half-life), mass spectrometer was operated in mixed HRMS/SWATH-MS/MS acquisition mode with total cycle time of 550 ms. To induce fragmentation, collision energy voltage (CE) was set to 35 V and collision energy spread voltage (CES) was set to 15 V.

To prepare degradation bar graph, peak area was represented in percentage as change relative to the value obtained just after mixing peptide with serum (0 h – 100%). GraphPad Prism Version-5.01 was used to present data and statistics. All results are represented as means ± SEM, determined from two independent experiments performed in duplicates.

4.5. Structural evaluation

4.5.1. Co-crystallization of compounds with $PvS1_{CD}$

Co-crystallization experiments were performed following the method described by Martinez *et al.* [19]. Initially, 1µL of inhibitor solution (5 mM in 50% DMSO) was transferred to a PCR tube and incubated at 37 °C for 24-48 hours to evaporate the DMSO. $PvS1_{CD}$ at 14 mg/mL was then mixed with the dried inhibitor (final protein:inhibitor ratio of 1:4.4) and incubated at 4 °C for 4 hours prior to setting up the crystallization drops. Initial crystals were obtained manually in Linbro plates using a hanging drop setup. Optimal crystals of $PvS1_{CD}$ in complex with inhibitors were obtained at 18 °C by mixing 1.5 µL of the protein complex with 1.5 µL of the reservoir solution containing 0.5 M $LiSO_4$ and 15% W/V PEG8000, and seeded with microcrystals (streak seeding) of $PvS1_{CD}$ grown in the absence of the inhibitor under the same crystallization conditions. Plate-like crystals appeared within 1-2 weeks, and single crystals were flash-frozen in liquid nitrogen using the mother liquor containing 1.25 mM of the respective inhibitor and 25% ethylene glycol as cryoprotectant prior to X-ray diffraction data collection.

4.5.2. X-ray data collection and 3D structure resolution

The diffraction data sets were collected from a single flash-frozen crystal at 100 K using beamlines ID29 and ID30 at ESRF (Grenoble, France) and Proxima-1 at SOLEIL synchrotron (Saint Aubin, France). These data were then processed with XDS [55] and scaled with AIMLESS from the CCP4 suite [56]. The crystal structures were solved by molecular replacement methods using Phaser software [57] and the catalytic domains of $PvS1_{FL}$ (pdb code 4TR2, residues Tyr_{277}-Lys_{611}) or of $PvS1_{CD}$ (pdb code 8COZ) as model probes. Structure refinement was carried out using BUSTER software [58], which incorporated TLS models and non-crystallographic symmetry restraints. Automatic TLS segmentation was performed with the TLSMD server. Manual rebuilding was performed using COOT [59]. The final data collection and refinement statistics are presented in Table S5, and the atomic coordinates and structure factors have been deposited in the Protein Data Bank with pdb codes 8QKG (compound **3**), 8QKJ (compound **7**), and 8QKE (compound **8**).

Declaration of competing interest

The authors declare that they have no competing financial interests or personal relationships that could have appeared to influence the work reported in this paper.

Acknowledgements.

This work was supported by *Institut Carnot Chimie Balard* (FO-ICCB-M1-08 V01), *Agence Nationale de la Recherche* (ANR-19-CE18-0010-01, including fellowship to FB, PA, AKP, LOV and AE). This project has also received funding from the European Union's Horizon 2020 research and innovation program under the Marie Sklodowska-Curie grant agreement SUBUN N° 898512 H2020-MSCA-IF-2019 (AKP). A. Bouillon and M. Martinez have been supported by *Agence Nationale pour la Recherche* (ANR-11-RPIB-002). LOV has also been supported by *Agence Nationale pour la Recherche* (ANR-17-CE11-0030) and by the "URGENCE COVID-19" fundraising campaign of Institut Pasteur.

We thank Mr Pierre Sanchez (IBMM, Montpellier, France) for mass spectrometry analyses. We thank the staff of the Crystallography core facility at the Institut Pasteur for carrying out robot-driven crystallization screenings. We acknowledge ESRF and SOLEIL for provision of synchrotron radiation facilities and we thank the staffs of the ID29, ID30 and Proxima-1 beamlines for support during data collection. We are grateful to the healthy volunteers for their contribution to the study and thank the staff, particularly Hélène Laude, Blanca Liliana Perlaza, Emmanuel Roux, Dorian Cheval, Linda Sangari and Sophie Vacant of ICAReB-Clin and ICAReB-biobank of the CRBIP (BioResource Center) from the Medical Direction at Institut Pasteur for managing the visits of healthy volunteers and for preparing and providing the human blood samples used to cultivate *P. falciparum*.

Appendix A. Supplementary data.

Supplementary data can be found online at…

Synthesis of special amino acids. Analysis and purification, Table S1 (characteristics of synthetic compounds **1-41**). Table S2 (inhibitory potencies of **1-41** against $PvS1_{CD}$). Table S3 (clogP values of selected compounds). Figure S1 (Inhibition of *P. falciparum* merozoite egress by compound **40**). Figure S2 (thermoshift assay). Figure S3 (elastase inhibition by compound **8**). Figures S4, S5 and Table S4 (stability of compounds **1** and **8** in human serum). Table S5, data collection and refinement statistics for crystallized complexes. Figure S6 (superposition of $PvS1_{CD}$ bound inhibitors). Figure S7 (electron density of $PvS1_{CD}$ bound inhibitors). Figure S8 (superimposition of $PvS1_{CD}$ binding pockets). Figure S9 (ligplot analysis). Chromatographic profiles of selected compounds from LC- or UPLC-MS analyses.

X-ray structures of SUB1/inhibitor complexes: pdb codes 8QKG (compound **3**), 8QKJ (compound **7**), 8QKE (compound **8**): Authors will release the atomic coordinates and experimental data upon article publication.

References.

[1] World Health Organization, Geneva (2022), World Malaria report, can be fund under https://www.who.int/teams/global-malaria-programme/reports/world-malaria-report-2022

[2] H. Noedl, Y. Se, K. Schaecher, B. L. Smith, D. Socheat, M. M. Fukuda; Artemisinin Resistance in Cambodia 1 (ARC1) Study Consortium, Evidence of artemisinin-resistant malaria in western Cambodia, N. Engl. J. Med. 359 (2008) 2619-2620. 10.1056/NEJMc0805011

[3] A. M. Dondorp, F. Nosten, P. Yi, D. Das, A. P. Phyo, J. Tarning, K. M. Lwin, F. Ariey, W. Hanpithakpong, S. J. Lee, P. Ringwald, K. Silamut, M. Imwong, K. Chotivanich, P. Lim, T. Herdman, S. S. An, S. Yeung, P. Singhasivanon, N. P. Day, N. Lindegardh, D. Socheat, N. J. White, Artemisinin resistance in *Plasmodium falciparum* malaria, N. Engl. J. Med. 361 (2009) 455-467. 10.1056/NEJMoa0808859

[4] A. Uwimama, E. Legrand, B. H. Stokes, J. M. Ndikumana, M. Warsame, N. Umulisa, D. Ngamije, T. Munyaneza, J. B. Mazarati, K. Munguti, P. Campagne, A. Criscuolo, F. Ariey, M. Murindahabi, P. Ringwald, D. A. Fidock, A. Mbituyumuremyi, D. Menard, Emergence and clonal expansion of *in vitro* artemisinin-resistant *Plasmodium falciparum* kelch13 R561H mutant parasites in Rwanda, Nat. Med. 26 (2020) 1602-1608. 10.1038/s41591-020-1005-2

[5] B. Balikagala, N. Fukuda, M. Ikeda, O. T. Katuro, S. I. Tachibana, M. Yamauchi, W. Opio, S. Emoto, D. A. Anywar, E. Kimura, N. M. Q. Palacpac, E. I. Odongo-Aginya, M. Ogwang, T. Horii, T. Mita, Evidence of artemisinin-resistant malaria in Africa, New Eng. J. Med. 385 (2021) 1163-1171. 10.1056/NEJMoa2101746

[6] M. Dhorda, C. Amaratunga, A. M. Dondorp, Artemisinin and multidrug-resistant *Plasmodium falciparum* - a threat for malaria control and elimination, Curr. Op. Inf. Dis. 34 (2021) 432-439. 10.1097/QCO.0000000000000766

[7] World Health Organization, Geneva (2023), Malaria threats map, can be fund under https://apps.who.int/malaria/maps/threats/

[8] M. J. Blackman, H. Fujioka, W. H. L. Stafford, M. Sajid, B. Clough, S. L. Fleck, M. Aikawai, M. Grainger, F. Hackett, A subtilisin-like protein in secretory organelles of *Plasmodium falciparum* merozoites, J. Biol. Chem. 273 (1998) 23398-23409. 10.1074/jbc.273.36.23398

[9] S. Yeoh, R. A. O'Donnell, K. Koussis, A. R. Dluzewski, K. H. Ansell, S. A. Osborne, F. Hackett, C. Withers-Martinez, G. H. Mitchell, L. H. Bannister, J. S. Bryans, C. A. Kettleborough, Michael J. Blackman, Subcellular discharge of a serine protease mediates release of invasive malaria parasites from host erythrocytes, Cell 131 (2007) 1072-1083. 10.1016/j.cell.2007.10.049

[10] L. Tawk, C. Lacroix, P. Gueirard, R. Kent, O. Gorgette, S. Thiberge, O. Mercereau-Puijalon, R. Ménard, J.-C. Barale, A key role for *Plasmodium* subtilisin-like SUB1 protease in egress of malaria parasites from host hepatocytes, J. Biol. Chem. 288 (2013), 33336-33346. 10.1074/jbc.M113.513234

[11] C. Suarez, K. Volkmann, A. R. Gomes, O. Billker, M. J. Blackman, The malarial serine protease SUB1 plays an essential role in parasite liver stage development, PloS Pathog. 9 (2013) e1003811. 10.1371/journal.ppat.1003811

[12] K. Koussis, C. Withers-Martinez, S. Yeoh, M. Child, F. Hackett, E. Knuepfer, L. Juliano, U. Woehlbier, H. Bujard, M. J Blackman, A multifunctional serine protease primes the malaria parasite for red blood cell invasion, EMBO J. 28 (2009) 725-735. 10.1038/emboj.2009.22

[13] T. Pace, F. Grasso, G. Camarda, C. Suarez, M. J. Blackman, M. Ponzi, A. Olivieri, The *Plasmodium berghei* serine protease PbSUB1 plays an important role in male gamete egress, Cell Microbiol. (2019) e13028. 10.1111/cmi.13028

[14] D. Leroy, B. Campo, X. C. Ding, J. N. Burrows, S. Cherbuin, Defining the biology component of the drug discovery strategy for malaria eradication, Trends Parasitol. 30 (2014) 478-490. 10.1016/j.pt.2014.07.004

[15] J. N. Burrows, S. Duparc, W. E. Gutteridge, R. Hooft van Huijsduijnen, W. Kaszubska, F. Macintyre, S. Mazzuri, J. J. Möhrle, T. N. C. Wells, New developments in anti-malarial target candidate and product profiles, Malar. J. 16 (2017) 26. 10.1186/s12936-016-1675-x

[16] J.-C. Barale, T. Blisnick, H. Fujioka, P. M. Alzari, M. Aikawa, C. Braun-Breton, G. Langsley, *Plasmodium falciparum* subtilisin-like protease 2, a merozoite candidate for the merozoite surface protein 1–42 maturase, Proc. Natl. Acad. Sci. USA 96 (1999) 6445-6450. 10.1073/pnas.96.11.6445

[17] A. Bouillon, D. Giganti, C. Benedet, O. Gorgette, S. Pêtres, E. Crublet, C. Girard-Blanc, B. Witkowski, D. Ménard, M. Nilges, O. Mercereau-Puijalon, V. Stoven, J.-C. Barale, In silico screening on the three-dimensional model of the *Plasmodium vivax* SUB1 protease leads to the validation of a novel anti-parasite compound, J. Biol. Chem. 288 (2013) 18561-18573. 10.1074/jbc.M113.456764

[18] C. Withers-Martinez, C. Suarez, S. Fulle, S. Kher, M. Penzo, J.-P. Ebejer, K. Koussis, F. Hackett, A. Jirgensons, P. Finn, M. J. Blackman, *Plasmodium* subtilisin-like protease 1 (SUB1): Insights into the active-site structure, specificity and function of a pan-malaria drug target, Int. J. Parasitol. 42 (2012) 597-612. 10.1016/j.ijpara.2012.04.005

[19] M. Martinez, F. Batista, M. Maurel, A. Bouillon, L. Ortega, A.-M. Wehenkel, L. Le Chevalier-Sontag, A. Blondel, A. Haouz, J.-F. Hernandez, P. M. Alzari, J.-C. Barale, 3D structures of the *Plasmodium vivax* SUB1 subtilisin-like drug target reveal conformational changes to accommodate a substrate-derived α-ketoamide inhibitor, Acta Crystallogr. D Biol. Crystallogr. D79 (2023) 721-734. 10.1107/S2059798323004710

[20] D. Giganti, A. Bouillon, L. Tawk, F. Robert, M. Martinez, E. Crublet, P. Weber, C. Girard-Blanc, S. Petres, A. Haouz, J.-F. Hernandez, O. Mercereau-Puijalon, P. M. Alzari, J.-C. Barale, A novel *Plasmodium*-specific prodomain fold regulates the malaria drug target SUB1 subtilase, Nat. Commun. 5 (2014) 4833. 10.1038/ncomms5833

[21] C. Withers-Martinez, M. Strath, F. Hackett, L. F. Haire, S. A. Howell, P. A. Walker, E. Christodoulou, G. G. Dodson, M. J. Blackman, The malaria parasite egress protease SUB1 is a calcium-dependent redox switch subtilisin, Nat. Commun. 5 (2014) 3726. 10.1038/ncomms4726

[22] S. Arastu-Kapur, E. L. Ponder, U. P. Fonovic, S. Yeoh, F. Yuan, M. Fonovic, M. Grainger, C. I. Phillips, J. C. Powers, M. Bogyo, Identification of proteases that regulate erythrocyte rupture by the malaria parasite *Plasmodium falciparum*, Nat. Chem. Biol. 4 (2008) 203-213. 10.1038/nchembio.70

[23] S. Gemma, S. Giovani, M. Brindisi, P. Tripaldi, S. Brogi, L. Savini, I. Fiorini, E. Novellino, S. Butini, G. Campiani, M. Penzo, M. J. Blackman, Quinolylhydrazones as novel inhibitors of *Plasmodium falciparum* serine protease PfSUB1, Bioorg. Med. Chem. Lett. 22 (2012) 5317-5321. 10.1016/j.bmcl.2012.06.023

[24] S. S. Kher, M. Penzo, S. Fulle, J. P. Ebejer, P. W. Finn, M. J. Blackman, A. Jirgensons, Quinoxaline-based inhibitors of malarial protease PfSUB1, Chem. Heterocycl. Compd. 50 (2015) 1456-1462. https://doi.org/10.1007/s10593-014-1610-4

[25] S. S. Kher, M. Penzo, S. Fulle, P. W. Finn, M. J. Blackman, A. Jirgensons, Substrate derived peptidic α-ketoamides as inhibitors of the malarial protease PfSUB1, Bioorg. Med. Chem. Lett. 24 (2014) 4486-4489. 10.1016/j.bmcl.2014.07.086

[26] S. Giovani, M. Penzo, S. Brogi, M. Brindisi, S. Gemma, E. Novellino, L. Savini, M. J. Blackman, G. Campiani, S. Butini, Rational design of the first difluorostatone-based PfSUB1 inhibitors, Bioorg. Med. Chem. Lett. 24 (2014) 3582-3586. 10.1016/j.bmcl.2014.05.044

[27] G. Bastianelli, A. Bouillon, C. Nguyen, E. Crublet, S. Pêtres, O. Gorgette, D. Le-Nguyen, J.-C. Barale, M. Nilges M, Computational reverse-engineering of a spider-venom derived peptide active against *Plasmodium falciparum* SUB1, PloS One 6 (2011) e21812. 10.1371/journal.pone.0021812

[28] G. Bastianelli, A. Bouillon, C. Nguyen, D. Le-Nguyen, M. Nilges, J.-C. Barale, Computational design of protein-based inhibitors of *Plasmodium vivax* subtilisin-like 1 protease, PLoS One 9 (2014) e109269. 10.1371/journal.pone.0109269

[29] E. Lidumniece, C. Withers-Martinez, F. Hackett, C. R. Collins, A. J. Perrin, K. Koussis, C. Bisson, M. J. Blackman, A. Jirgensons, Peptidic boronic acids are potent cell-permeable inhibitors of the malaria parasite egress serine protease SUB1, Proc. Natl. Acad. Sci. USA 118 (2021) e2022696118. 10.1073/pnas.2022696118

[30] E. Lidumniece, C. Withers-Martinez, F. Hackett, M. J. Blackman, A. Jirgensons, Subtilisin-like serine protease 1 (SUB1) as an emerging antimalarial drug target: current achievements in inhibitor discovery, J. Med. Chem. 65 (2022) 12535-12545. 10.1021/acs.jmedchem.2c01093

[31] N. D. Rawlings, A. J. Barrett, P. D. Thomas, X. Huang, A. Bateman, R. D. Finn, The MEROPS database of proteolytic enzymes, their substrates and inhibitors in 2017 and a comparison with peptidases in the PANTHER database, Nucleic Acids Res. 46 (2018) D624-D632. 10.1093/nar/gkx1134

[32] M. Robello, E. Barresi, E. Baglini, S. Salerno, S. Taliani, F. Da Settimo, The alpha keto amide moiety as a privileged motif in medicinal chemistry: current insights and emerging opportunities, J. Med. Chem. 64 (2021) 3508-3545. 10.1021/acs.jmedchem.0c01808

[33] E. D. Putrianti, A. Schmidt-Christensen, V. Heussler, K. Matuschewski, A. Ingmundson, A *Plasmodium* cysteine protease required for efficient transition from the liver infection stage, PLoS Pathog. 16 (2020) e1008891. 10.1371/journal.ppat.1008891

[34] T. D. Schneider, R. M. Stephens, Sequence logos: a new way to display consensus sequences, Nucleic Acids Res. 18 (1990) 6097-6100. 10.1093/nar/18.20.6097

[35] G. E. Crooks, G. Hon, J. M. Chandonia, S. E. Brenner, WebLogo: a sequence logo generator, Genome Res. 14 (2004) 1188-1190. 10.1101/gr.849004

[36] F. Rohrbacher, A. Zwicky, J. W. Bode, Facile synthesis of internal and C-terminal peptide α-ketoamides with Fmoc-solid phase peptide synthesis, Helv. Chim. Acta 101 (2018) e1800039. https://doi.org/10.1002/hlca.201800039

[37] R. J. Herr, 5-Substituted-1*H*-tetrazoles as carboxylic acid isosteres: medicinal chemistry and synthetic methods, Bioorg. Med. Chem. 10 (2002) 3379-3393. 10.1016/s0968-0896(02)00239-0

[38] V. V. Sureshbabu, R. Venkataramanarao, S. A. Naik, G. Chennakrishnareddy, Synthesis of tetrazole analogues of amino acids using Fmoc chemistry: isolation of amino free tetrazoles and their incorporation into peptides, Tetrahedron Lett. 48 (2007) 7038-7041. https://doi.org/10.1016/j.tetlet.2007.07.129

[39] P. L. Ornstein, D. D. Schoepp, M. B. Arnold, J. D. Leander, D. Lodge, J. W. Paschal, T. Elzey, 4-(Tetrazolylalkyl)piperidine-2-carboxylic acids. Potent and selective *N*-methyl-D-aspartic acid receptor antagonists with a short duration of action, J. Med. Chem. 34 (1991) 90-97. 10.1021/jm00105a016

[40] N. R. Penthala, S. Bommagani, J. Yadlapalli, P. A. Crooks, A novel and efficient tributyltin azide-mediated synthesis of 1*H*-tetrazolylstilbenes from cyanostilbenes, Tetrahedron Lett. 57 (2016) 1807-1810. https://doi.org/10.1016/j.tetlet.2016.03.040

[41] A. Bouillon, O. Georgette, O. Mercereau-Puijalon, J.-C. Barale, Screening and evaluation of inhibitors of *Plasmodium falciparum* merozoite egress and invasion using cytometry, Methods Mol. Biol. 923 (2013) 523-534. 10.1007/978-1-62703-026-7_36

[42] C.-L. Ciana, R. Siegrist, H. Aissaoui, L. Marx, S. Racine, S. Meyer , C. Binkert, R. de Kanter , C. Fischli, S. Wittlin, C . Boss, Novel *in vivo* active anti-malarials based on a hydroxy-ethyl-amine scaffold, Bioorg. Med. Chem. Lett. 23 (2013) 658-662. 10.1016/j.bmcl.2012.11.118

[43] P. Pino, R. Caldelari, B. Mukherjee, J. Vahokoski, N. Klages, B. Maco, C. R. Collins, M. J. Blackman, I. Kursula, V. Heussler, M. Brochet, D. Soldati-Favre, A multistage antimalarial targets the plasmepsins IX and X essential for invasion and egress, Science 358 (2017) 522-528. 10.1126/science.aaf8675

[44] N. C. Silmon de Monerri, H. R. Flynn, M. G. Campos, F. Hackett, K. Koussis, C. Withers-Martinez, J. M. Skehel, M. J. Blackman, Global identification of multiple substrates for *Plasmodium falciparum* SUB1, an essential malarial processing protease, *Infect. Immun*. 79 (2011) 1086-1097. 10.1128/IAI.00902-10

[45] P. Singh, K. Samanta, N. M. Kebe, G. Michel, B. Legrand, V. E. Sitnikova, A. V. Kajava, M. Pagès, P. Bastien, C. Pomares, O. Coux, J.-F. Hernandez, The C-terminal segment of *Leishmania*

major HslU: Toward potential inhibitors of LmHslVU activity, Bioorg. Chem. 119 (2021) 105539. 10.1016/j.bioorg.2021.105539

[46] C. Ballatore, D. M. Huryn, A. B. Smith III, Carboxylic acid (bio)isosteres in drug design, ChemMedChem 8 (2013) 385-395. 10.1002/cmdc.201200585

[47] P. Lassalas, B. Gay, C. Lasfargeas, M. J. James, Van Tran, K. G. Vijayendran, K. R. Brunden, M. C. Kozlowski, C. J. Thomas, A. B. Smith III, D. M. Huryn, C. Ballatore, Structure property relationships of carboxylic acid isosteres, J. Med. Chem. 59 (2016) 3183-3203. 10.1021/acs.jmedchem.5b01963

[48] W. S. Hancock, J. E. Battersby, A new micro-test for the detection of incomplete coupling reactions in solid-phase peptide synthesis using 2,4,6-trinitrobenzenesulphonic acid, Anal. Biochem. 71 (1976) 260-264. 10.1016/0003-2697(76)90034-8

[49] R. B. Perni, S. J. Almquist, R. A. Byrn, G. Chandorkar, P. R. Chaturvedi, L. F. Courtney, C. J. Decker, K. Dinehart, C. A. Gates, S. L. Harbeson, A. Heiser, G. Kalkeri, E. Kolaczkowski, K. Lin, Y. P. Luong, B. G. Rao, W. P. Taylor, J. A. Thomson, R. D. Tung, Y. Wei, A. D. Kwong, C. Lin, Preclinical profile of VX-950, a potent, selective, and orally bioavailable inhibitor of hepatitis C virus NS3-4A serine protease, Antimicrob. Agents Chemother. 50 (2006) 899-909. 10.1128/AAC.50.3.899-909.2006

[50] R. A. Copeland. Tight binding inhibition. In "Evaluation of enzyme inhibitors in drug discovery: A guide for medicinal chemists and pharmacologists", 2nd Edition. Wiley (2005) 245-282.

[51] J. F. Morrison, Kinetics of the reversible inhibition of enzyme-catalysed reactions by tight-binding inhibitors, Biochim. Biophys. Acta 185 (1969) 269-286. 10.1016/0005-2744(69)90420-3

[52] J. Lainé, M. Beattie, D. LeBel, Simultaneous kinetic determinations of lipase, chymotrypsin, trypsin, elastase, and amylase on the same microtiter plate, Pancreas 8 (1993) 383-386. 10.1097/00006676-199305000-00016

[53] P. Esterre, A. Ait-Saadi, L. Arowas, S. Chaouche, N. Corre-Catelin, C. Fanaud, H. Laude, V. Mellon, V. Monceaux, G. Morizot, I. Najjar, C. Ottone, B. L. Perlaza, B. Rimbault, L. Sangari, M.-N. Ungeheuer,. The ICAReB Platform: A human biobank for the Institut Pasteur and beyond, Open J. Biores. 7 (2020) 1. DOI: 10.5334/ojb.66

[54] A. K. Puszko, P. Sosnowski, R. Rignault-Bricard, O. Hermine, G. Hopfgartner, K. Pułka-Ziach, Y. Lepelletier, A. Misicka, Urea-peptide hybrids as VEGF-A_{165}/NRP-1 complex inhibitors

with improved receptor affinity and biological properties, Int. J. Mol. Sci. 22 (2020) 72. 10.3390/ijms22010072

[55] W. Kabsch, XDS, Acta Crystallogr. D Biol. Crystallogr. 66 (2010) 125-132. 10.1107/S0907444909047337

[56] Collaborative Computational Project, Number 4, The CCP4 suite: programs for protein crystallography, Acta Crystallogr. D Biol. Crystallogr. 50 (1994) 760-763. 10.1107/S0907444994003112

[57] A. J. McCoy, R. W. Grosse-Kunstleve, P. D. Adams, M. D. Winn, L. C. Storoni, R. J. Read, Phaser crystallographic software, J. Appl. Crystallogr. 40 (2007) 658-674. 10.1107/S0021889807021206

[58] G. Bricogne, E. Blanc, M. Brandl, C. Flensburg, P. Keller, W. Paciorek, P. Roversi, O. S. Smart, C. Vonrhein, T. O. Womack, Buster (2009) Version 2.9.3. Cambridge, UK: Global Phasing Ltd.

[59] P. Emsley, B. Lohkamp, W. G. Scott, K. Cowtan, Features and development of Coot, Acta Crystallogr. D Biol. Crystallogr. 66 (2010) 486-501. 10.1107/S0907444910007493